Doctoral Thesis

Development of ^{68}Ga-Labeled Multivalent Nitroimidazole Derivatives for Hypoxia Imaging

August 2016

Graduate School of Seoul National University

Natural Science

Interdisciplinary Program in Radiation Applied Life Science

Seelam Sudhakara Reddy

이학박사학위논문

Development of ^{68}Ga-Labeled Multivalent Nitroimidazole Derivatives for Hypoxia Imaging

저산소 영상을 위한 ^{68}Ga-표지 다가(多價) 나이트로이미다졸 유도체 개발

2016 년 8 월

서울대학교대학원

협동과정 방사선응용생명과학 전공

Seelam Sudhakara Reddy

저산소 영상을 위한 ^{68}Ga-표지 다가(多價) 나이트로이미다졸 유도체 개발

지도교수 정재민

이 논문을 이학박사 학위논문으로 제출함

2016 년 4 월

서울대학교대학원

협동과정 방사선응용생명과학 전공

Seelam Sudhakara Reddy

Seelam Sudhakara Reddy 의 이학박사 학위논문으로 인준함

2016 년 6 월

위 원 장 예 성 준 (Seal)

부위원장 정 재 민 (Seal)

위 원 이 계 성 (Seal)

위 원 최 연 성 (Seal)

위 원 (Seal)

Development of ^{68}Ga-Labeled Multivalent Nitroimidazole Derivatives for Hypoxia Imaging

(Academic Advisor: Jae Min Jeong, Ph.D)

Submitting a Doctoral Thesis in Natural Science

April 2016

Graduate School of Seoul National University

Natural Science

Interdisciplinary Program in Radiation Applied Life Science

Seelam Sudhakara Reddy

Confirming the Doctoral Thesis Written by

Mr. Seelam Sudhakara Reddy

June 2016

Chair Sung-Joon Ye (Seal)

Vice Chair Jae Min Jeong (Seal)

Examiner Jae Sung Lee (Seal)

Examiner Yearn Seong Choe (Seal)

Examiner Ji Seong Choon (Seal)

Abstract

Development of ^{68}Ga-Labeled Multivalent Nitroimidazole Derivatives for Hypoxia Imaging

Seelam Sudhakara Reddy

Department of Nuclear Medicine

Interdisciplinary Program in Radiation Applied Life Science

The Graduate School

Seoul National University College of Medicine

Radiolabeled nitroimidazole (NI) derivatives have been extensively studied for imaging hypoxia. To increase the hypoxic tissue uptake, we developed ^{68}Ga-labeled agents based on mono-, bis-, and trisnitroimidazole conjugates with the chelating agent 1,4,7-triazacyclononane-1,4,7-tris[methyl(2-carboxyethyl)phosphinic acid] (TRAP). All the three agents showed high radiolabeling yields (>96%) and were found to be stable up to 4 h in prepared medium at room temperature and in human serum at 37 °C. The trivalent agent showed a significant increase in hypoxic to normoxic uptake ratio ($p < 0.005$) according to the in vitro cell uptake experiments. Immunohistochemical analysis confirmed the presence of hypoxia in xenografted CT26 tumor tissue. The trivalent derivative (^{68}Ga-**3**: 0.17 ± 0.04,

^{68}Ga-**4**: 0.33 ± 0.04, ^{68}Ga-**5**: 0.45 ± 0.09, and ^{68}Ga-**6**: 0.47 ± 0.05% ID/g) showed the highest uptake by tumor cells according to the biodistribution studies in CT-26 xenografted mice. All the nitroimidazole derivatives showed significantly higher uptake by tumor cells than the control agent ($p < 0.05$) at 1 h post-injection. The trivalent derivative (^{68}Ga-**3**: 0.10 ± 0.06; ^{68}Ga-**4**: 0.20 ± 0.06; ^{68}Ga-**5**: 0.33 ± 0.08; ^{68}Ga-**6**: 0.59 ± 0.09) also showed the highest standard uptake value for tumor cells at 1 h post-injection in animal PET studies using CT-26 xenografted mice. In conclusion, we successfully synthesized multivalent ^{68}Ga-labeled NI derivatives for imaging hypoxia. Among them, the trivalent agent showed the highest tumor uptake in biodistribution and animal PET studies.

Keywords: trisnitroimidazole; bisnitroimidazole; multidentate; gallium-68; hypoxia; PET.

Student number: 2010-31372

Contents

List of Tables

List of Figures

values show comparisons of uptake under normoxic and hypoxic conditions (*t*-test): (**) $p < 0.005$, (*) $p < 0.05$, $n = 3$ at each time point.

Figure 10. Immunohistochemical staining of CT26 tumor xenografts to detect hypoxia. Tumor tissue was obtained from xenografted mice at 1.5 h after intravenous injection of Hypoxyprobe^{TM}-1. Hypoxic lesions are shown in brown. (A) 40× and (B) 100× magnification images.

Figure 11. Small animal PET images of ^{68}Ga-labeled nitroimidazole derivatives. Images of mice bearing colon cancer CT-26 xenografts were recorded at (A) 1 h post-injection (23 MBq/0.1 ml per mouse via the tail vein). SUVs obtained after (B) 1 h and post-injection from animal PET images.

List of Synthetic Scheme

1. Introduction

Radiolabeled nitroimidazole derivatives are used for imaging hypoxic tissue because the nitroimidazole residue is reduced to reactive chemical species that can bind to intracellular components in the absence of sufficient oxygen [1-5].

In particular, 2-nitroimidazole can be reduced to form a reactive chemical species, which can bind to cell components in the absence of sufficient oxygen, and thus, the development of radio labeled nitroimidazole derivatives for the imaging of hypoxia remains an active field of research to improve cancer therapy result. When a nitroimidazole enters hypoxic cells, the molecule undergoes an enzymatic single electron reduction depending on availability of oxygen which forms a radical anion [6]. In the presence of normal oxygen levels the molecule is immediately reoxidized (Figure 1). This futile shuttling takes place for some time, before the molecule diffuses out of the cell. In hypoxic tissue the low oxygen concentration is not able to effectively compete to reoxidize the molecule and further reduction appears to take place, culminating in the association of the reduced nitroimidazole with various intracellular components. The association is not irreversible, since these agents clear from hypoxic tissue over time. The radical anion appears to undergo additional reduction and binds to macromolecules, and thus the associated radiolabel is selectively retained in hypoxic cells. This under

hypoxic conditions, bioreductive metabolism leads to further stepwise reduction of 1-e^- reduction product to nitroso ($2e^-$), hydroxylamine ($4e^-$) and amine ($6e^-$) derivatives (Figure 2). Labeled nitroimidazole derivatives are therefore potential radiopharmaceuticals for imaging hypoxic areas. So, development of radiolabeled derivatives of nitroimidazole for hypoxia imaging remains an active field of research for a better clinical outcome.

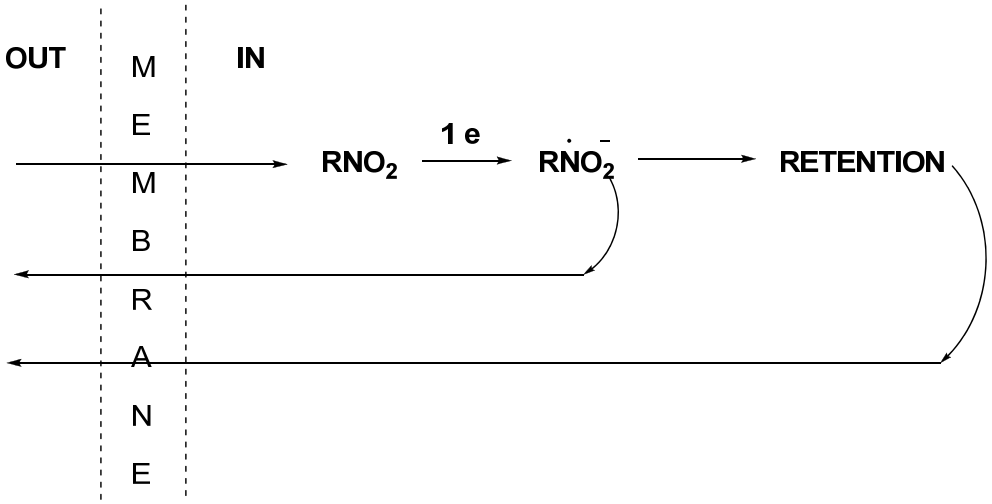

Figure 1. proposed mechanism for loss of nitroimidazole from well oxygenated tissue.

Halogenated nitroimidazole, such as [^{18}F]fluoromisonidazole ([^{18}F]FMISO, Figure 3) [7-9], [^{18}F] 1-α-D-(2-deoxy-2-fluoroarabinofuranosyl)-2-nitroimidazole ([^{18}F]FAZA) [10-13] and [^{123}I] 1-(5-iodo-5-deoxy-ß-D-arabinofuranosyl)-2-nitroimidazole (iodoazomycin arabinoside) ([^{124}I]IAZA) [14] have been used clinically to detect hypoxia in tumors. [^{18}F]FMISO is the first and well known nitroimidazole agent used for imaging hypoxia. However it is rather lipophilic, which may contribute to the finding that hypoxia specific accumulation is rather slow. The need to wait several hours to permit clearance of the agent from the normoxic background tissue (contrast between lesion and and background typically < 2:1 at about 90 min after injection), which is a serious fault to ^{18}F labeled agents having a relatively short half-life (110 min). Therefore, a continuous attempt to develop more feasible compounds for clinical use is in progress. One such candidate is fluorine-18 labeled fluoroerythronitroimidazole ([^{18}F]FETNIM) [15], which is a more hydrophilic nitroimidazole compound and shows rapid elimination of non-target tissues via excretion through the urinary pathway. [^{18}F]1-R-D-(2-deoxy-2-fluoroarabinofuranosyl)-2-nitroimidazole ([^{18}F]FAZA) [10-13], 2-(2-nitroimidazol-1-yl)-*N*-(3,3,3-[^{18}F]-trifluoropropyl)acetamide, ([^{18}F]EF-3) [16], [^{18}F]2-(2-nitro-1H-imidazol-1-y1)-N-(2,2,3,3,3-pentafluoropropyl) acetamide (([^{18}F]EF-5) [17-20], 3-[^{18}F]fluoro-2-(4-((2-nitro-1*H*-imidazol-1-yl)methyl)-1*H*-1,2,3,-triazol-1-yl)-propan-1-ol ([^{18}F]HX-4) [21],

fluoroetanidazole ([^{18}F]FETA) [22], 1-[^{18}F]Fluoro-3-(3-nitro-1H-1,2,4-triazol-1-yl)propan-2-ol ([^{18}F]NEFA), 2-[^{18}F]Fluoro-N-(2-(2-nitro-1H-imidazol-1-yl)ethyl)acetamide ([^{18}F]NEFT) [23], 3-[^{18}F]Fluoro-2-(4-((2-nitro-1H-imidazol-1-yl)methyl)-1H-1,2,3-triazol-1-yl)propan-1-ol ([^{18}F]3-NTR) [28] and [^{124}I]1-R-D-(2-deoxy- 2-fluoroarabinofuranosyl)-2-nitroimidazole ([^{124}I]IAZA) [14] are other known hypoxia imaging agents (Figure 3) developed to improve the imaging performance by improving target to non-target ratio by increasing excretion rates. However, the production of these radioisotopes is limited on cyclotron chemistry processing system which is expensive as well as difficult to handle. This has led to a great interest in the development of ^{68}Ga-labeled analogues which would be less expensive and more convenient to use.

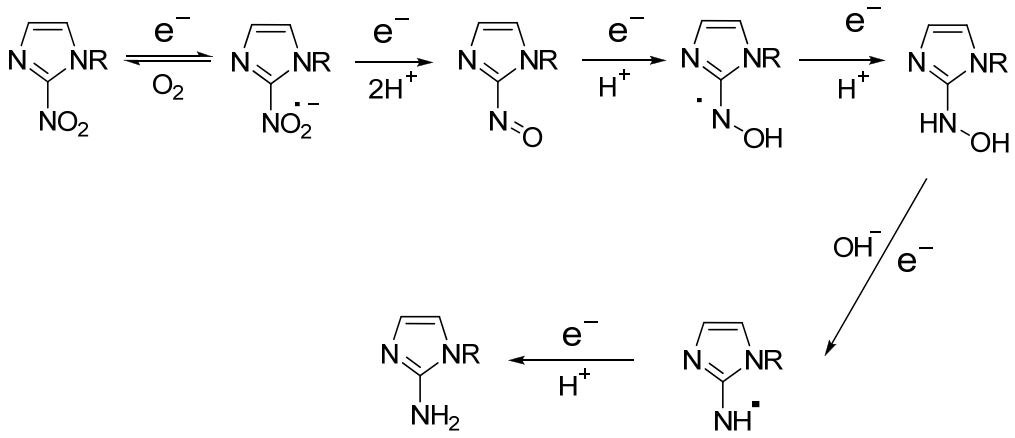

Figure 2. Proposed mechanism for nitroimidazole.

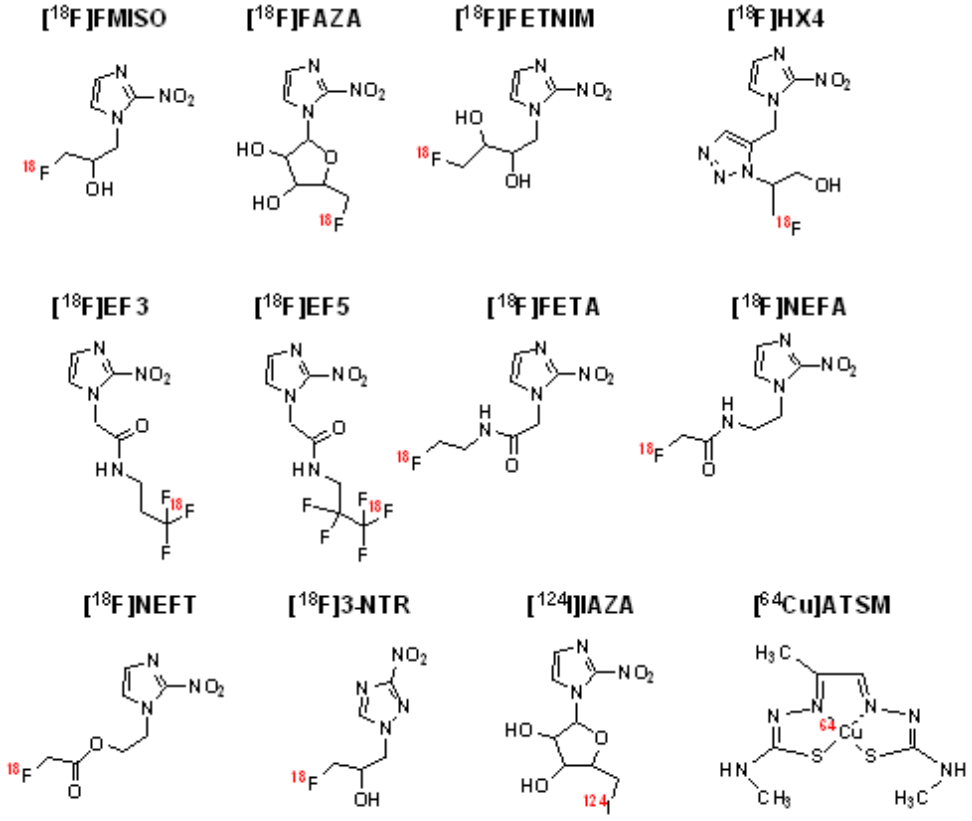

Figure 3. Known nitroimidazole agents for imaging hypoxia.

Furthermore ^{64}Cu-diacetyl-bis(N4-methylthiosemicarbazone) (ATSM) [25, 26] and ^{60}Cu-ATSM [25, 27] have been developed, showing faster clearance rate from normoxic tissue allows a shorter waiting time between administration and imaging. The PET images of ^{60}Cu-ATSM showing a hypoxic tumor (tumor-to-muscle ratio=3.1) and a normoxic tumor (tumor to muscle-to-muscle ratio=2.3) can be seen in Figure 4. The tumor has increased tracer uptake compared with surrounding tissues because the ^{60}Cu-ATSM is reduced and retained more avidly in hypoxic tissues [28]. However the production of ^{60}Cu and ^{64}Cu requires a special solid target and expensive target material, and hence, its use is likely to be limited. In fact, the productions of ^{18}F, ^{64}Cu, and ^{124}I require a cyclotron and chemical processing, which are expensive and difficult to operate and maintain.

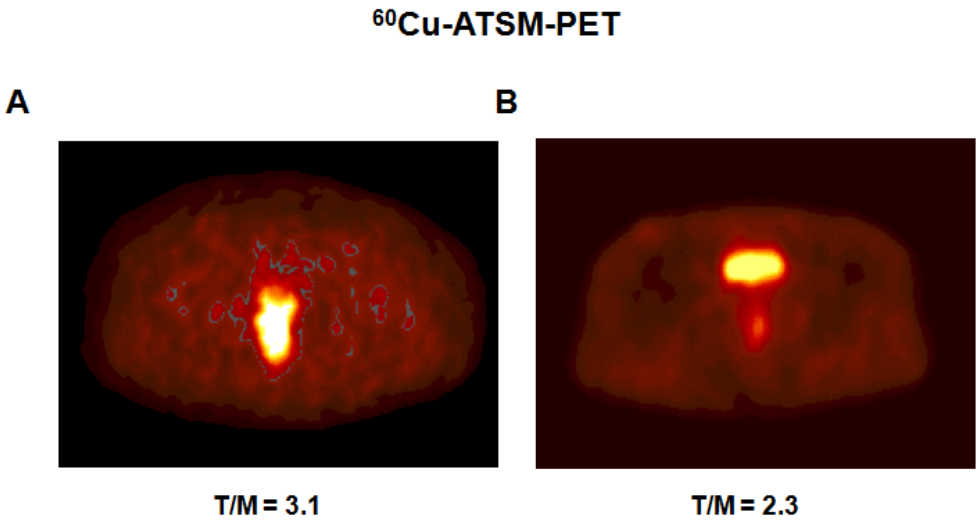

Figure 4. (A) ^{60}Cu-ATSM-positron emission tomography scan showing a hypoxic tumor. (B) ^{60}Cu-ATSM-positron emission tomography scan showing a normoxic tumor. The bright spot above the tumor is the bladder. Reprinted by permission of the Springer from: Dietz, D W., et al., Diseases of the Colon & Rectum, 2008;51(11):1641-8.

Positron emission tomography (PET) is a nuclear imaging technique applied for diagnosis of various types of cancers such as colorectal cancer, melanoma, head & neck cancer, lung cancer, breast cancer, prostate cancer, and so on, due to its wide scope and high sensitivity [8, 29-34]. ^{68}Ga ($t_{1/2}$ = 68 min, 89% β+, $E_{\beta+max}$ = 1.92 MeV, 11% EC) is a generator-produced radionuclide that offers excellent coordination chemistry with a wide range of bifunctional chelating agents. It also provides rapid radiolabeling in various pH ranges [35-42].

For preparing ^{68}Ga-labeled radiopharmaceuticals, 1,4,7-triazacyclononane-1,4,7-triacetic acid (NOTA, **1**, Figure 5) is one of the most commonly used bifunctional chelating agents due to its commercial availability and its formation an extremely stable six-coordinate Ga complex with high thermodynamic stability [43]. The bifunctional chelating agents like 1,4,7-triazacyclononane-1,4,7-triaceticacid (NOTA,) [44] and 1,4,7,10-tetraazacyclododecane-1,4,7,10-tetraacetic acid (DOTA) [45] have been most widely utilized which shows good conformational and size selectively towards small cation like Ga^{3+} with higher stability and easy availability. Especially the triazamacrocyclic ligand, NOTA, has been reported to form highly stable complexes with small cations like Ga^{3+}, and thus, various peptides conjugated with NOTA derivatives have been developed. NOTA has six coordinating

donor atoms with three nitrogens and three oxygens and DOTA has eight coordinating donor atoms with four nitrogens and four oxygens.

Due to the commercial availability of NOTA and DOTA derivatives, these are extensively used for conjugational chemistry related to medical imaging, including ^{68}Ga applications [36, 46, 47]. Actually, NOTA-based ligands showed higher selectivity towards Ga^{3+} ion and their complexes are more stable, as the size of the NOTA cavity is almost ideal for this ion [40, 48]. However, application of NOTA for a targeted PET probe design is restricted because of its limited bifunctionality. The coordinating ability of the NOTA with ^{68}Ga is compromised due to the loss of a coordinating pendant carboxylate group after conjugation with a targeting vector with it. Therefore, NOTA derivatives containing a linker, such as 2-(4-isothiocyanatobenzyl)-1,4,7-triazacyclononane-1,4,7 triaceticacid (p-SCN-Bn-NOTA) and 2-(4,7-bis-(carboxymethyl)-1,4,7-triazonan-1-yl)pentanedioic acid (NODAGA), 1,4,7-triazacyclononane-1,4-bis[methylene(hydroxymethyl)phosphinic acid]-7-[methylene(2-carboxyethyl)phosphinic acid] (NOPO) have been designed to avoid this problem [36, 49-52].

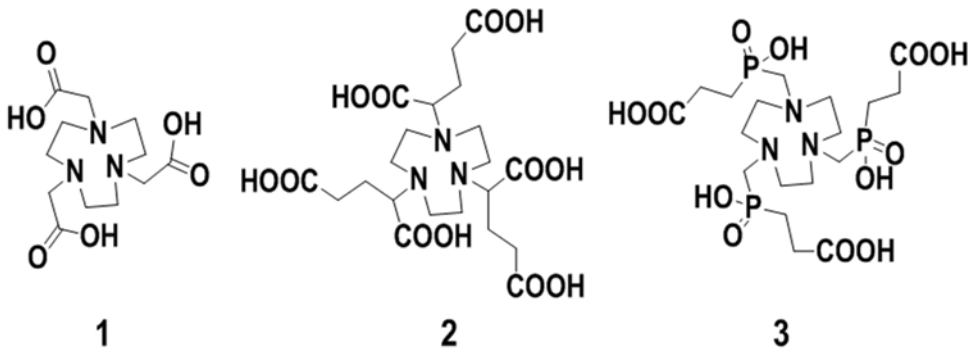

Figure 5. Structures of NOTA (**1**), NOTGA (contains glutaric acids), (**2**) and TRAP (contains phosphinic acids) (**3**).

Although nitroimidazole derivatives conjugated with 1,4,7,10-tetraazacyclododecane-1,4,7,10-tetraacetic acid (DOTA) for ^{68}Ga labeling have been reported, NOTA-nitroimidazole conjugates have shown higher tumor-to-muscle standard uptake value (SUV) ratios than DOTA-nitroimidazole derivatives [53, 54]. ^{18}F-labeled 1,4,7-triazacyclononane-1,4-diacetic acid (NODA)-nitroimidazole derivatives have been reported and these conjugates showed the higher SUVs and tumor-to-muscle ratios than NOTA and DOTA nitroimidazole derivatives (Figure 6) [55].

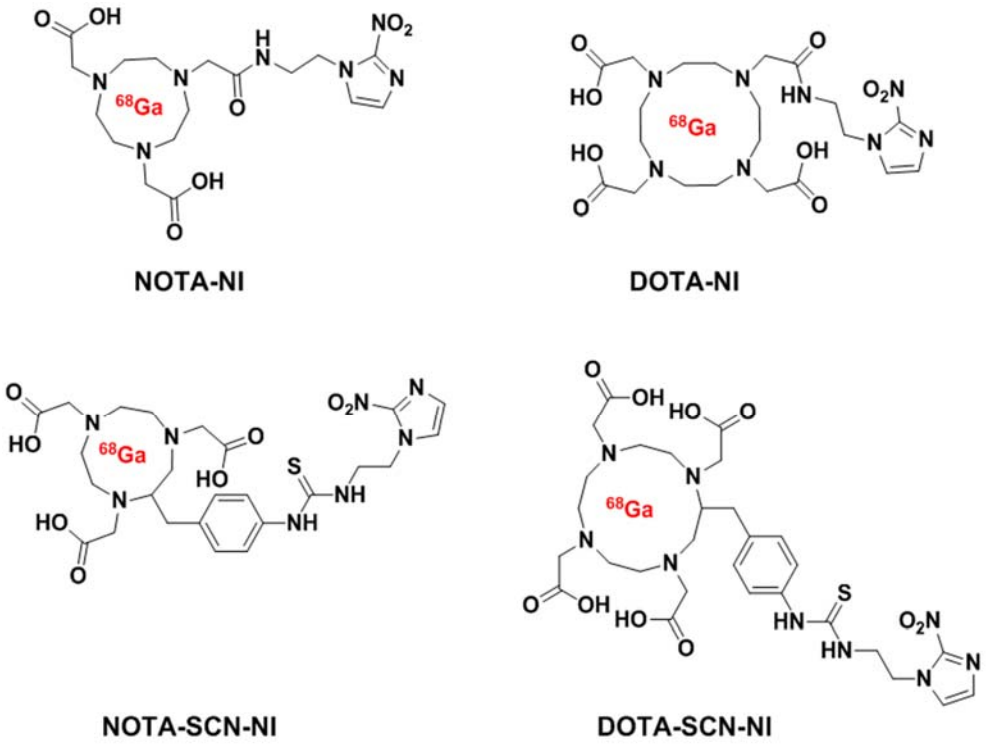

Figure 6. Structures of ^{68}Ga labeled nitroimidazole derivatives which were developed recently.

The above-reported derivatives contain only one nitroimidazole residue per molecule. Bisnitroimidazole derivatives labeled with ^{99m}Tc have been reported and showed improved biodistribution [56, 57]. Multivalent effect was used for increasing the uptake of nitroimidazole derivatives. Generally, a multimeric ligand enhances its local concentration on the cell surface thus increase the feasibility of the specific ligand-receptor interaction, which results in enhanced affinity and target accumulation [47]. Nitroimidazole derivatives are trapped inside cells in hypoxic condition after formation of reactive species. If a molecule has two or more nitroimidazole moieties, then it would be trapped in the hypoxic cells with higher probability. Recent attention in ligand design has been focused on studying and optimising chelators N-functionalised with three pendant arms containing sites for both coordination and conjugation, and developed 1,4,7-triazacyclononane-1,4,7-triglutaric acid (NOTGA, **2**, Figure 5) or 1,4,7-triazacyclononane-1,4,7-tris[methyl(2-carboxyethyl)phosphinic acid] (TRAP, **3**, Figure 5) for multivalent conjugation of ligands to the three pendant arms and ^{68}Ga labeling (Figure 5) [47, 48, 58] . Compared to the other ligands, synthesis of TRAP is more simple, fast and scalable. Moreover, protection is not required before conjugation with ligands by amide formation [48, 58]. Another advantage of the phosphinate based chelators is phosphonate donating groups are much less susceptible to transmetalation when compared with acetic acid donors. The

above studies has been used to form trimeric bioconjugate species although keeping the coordinating atoms for ^{68}Ga radiolabeling. Further studies showed that ^{68}Ga-labeled trivalent derivatives of TRAP and NODGA derivatives have higher binding affinity and tumor accumulation than their monovalent and bivalent counterparts [47, 48, 58-60].

In the present study, we attempted to develop a series of TRAP-based nitroimidazole derivatives, such as 3-((7-mono((hydroxy(3-(2-(2-nitroimidazolyl)ethylamino)-3-oxopropyl)phosphoryl)methyl)-1,4,7-triazonane -1,4-[methyl(2-carboxyethyl)phosphinic acid] (**4**), 3-(((4,7-bis((hydroxy(3-(2-(2-nitroimidazolyl)ethylamino)-3-oxopropyl)phosphoryl)methyl)-1,4,7-triazonane -1-[methyl(2-carboxyethyl)phosphinic acid] (**5**), and 1,4,7-triazonane-1,4,7-triyl(tris(methylene)tris(3-(2-(2-nitroimidazolyl)ethylamino)-3-oxopropylphosphinic acid (**6**) by conjugation of 2-(2-nitroimidazolyl)ethylamine hydrochloride with **3** to be used as ^{68}Ga-based hypoxia PET probe (Scheme 1).

Scheme 1. Synthesis of **4**, **5** and **6**[a]

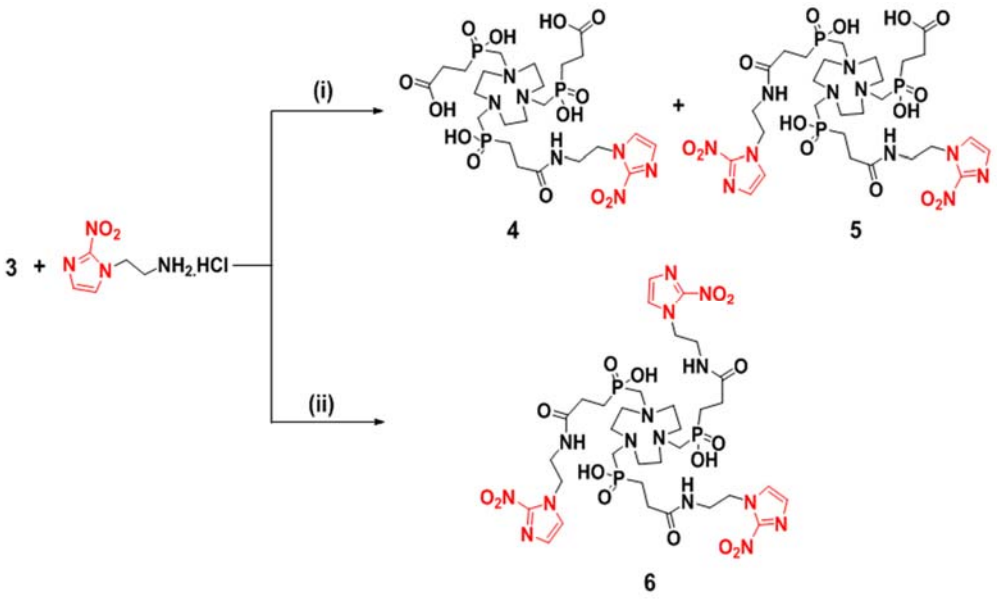

[a] Reagents and conditions: (i) **3** (0.2 mmol), 2-(2-nitroimidazolyl)ethylamine hydrochloride (1.1 mmol), HBTU (1.3 mmol), DIPEA (1.5 mmol), and DMSO (8 mL); (ii) **3** (0.1 mmol), 2-(2-nitroimidazolyl)ethylamine hydrochloride (1.0 mmol), HBTU (1.2 mmol), DIPEA (1.2 mmol), and DMSO (2 mL).

2. Materials and methods

2-1. General

1,4,7-triazacyclononane was purchased from ChemaTech (Dijon, France). All other chemicals were purchased from Sigma/Aldrich (St. Louis, MO, U.S.A.). The $^{68}Ge/^{68}Ga$-generator was purchased from Isotope Technologies Garching GmbH (Garching, Germany). ^{1}H, ^{13}C, and ^{31}P NMR spectra were recorded using a Brucker Avance 600 FT NMR spectrometer (600 MHz for ^{1}H, 150 MHz for ^{13}C, and 242 MHz for ^{31}P; Brucker Ltd., Germany). Chemical shifts (δ) were reported in ppm downfield from tetramethylsilane and multiplicities are indicated by s (singlet), d (doublet), t (triplet), m (multiplet), and br (broad). Electrospray ionization positive mode mass spectra (ESI^{+}-MS) were acquired on a Waters ESI ion trap spectrometer (Milford, MA, U.S.A.). The samples were diluted 1 to 100 times with methanol and injected directly into the injection port. Data are reported in the form of (*m/z*) versus intensity. HRMS were acquired on a LTQ-Orbitrap Velos ion trap spectrometer (Thermo Scientific, France). HPLC was performed using an XTerra RP18 (10 mm × 250 mm) and RP18 (4.5 mm × 100 mm) columns from Waters Corporation (Milford, MA, U.S.A.). The solvent systems used were A (10 mM HCl in H_2O) and B (MeCN), and the flow rates for analytical and preparative HPLC were 1 and 5 mL/min with the suggested linear gradients, respectively. The purities of the synthesized compounds were confirmed to be higher than

99% by analytical HPLC (Supporting Information). A Packard Cobra II (Global Market Institute, MN, U.S.A.) gamma scintillation counter was used to measure the radioactivity. The labeling yield was determined by Instant Thin-Layer Chromatography (ITLC SG; Varian, Agilent Technologies (Lake Forest City, CA, U.S.A.) in 0.1 M Na_2CO_3 solution. The strip was counted using a TLC scanner (AR-2000; Bioscan, U.S.A.). PET images were obtained using a small-animal PET scanner from GE Healthcare (Princeton, NJ, U.S.A.).

All animal experiments were performed with the approval of the Institutional Animal Care and Use Committee of the Biomedical Research Institute at Seoul National University Hospital (a facility accredited by the Association for Assessment and Accreditation of Laboratory Animal Care). In addition, the National Research Council guidelines for the care and use of laboratory animals (revised in 1996) were observed throughout.

2-2. Chemical synthesis

2-2-1. 3-((7-mono ((hydroxy(3-(2-(2-nitroimidazolyl)ethylamino)-3-oxopropyl)phosphoryl)methyl)-1,4,7-triazonane -1,4-[methyl(2-carboxyethyl)phosphinic acid] (4) and 3-(((4,7-bis((hydroxy(3-(2-(2-nitroimidazolyl)ethylamino)-3-oxopropyl)phosphoryl)methyl)-1,4,7-triazonane -1-[methyl(2-carboxyethyl)phosphinic acid] (5).

N,N-Diisopropylethylamine (DIPEA, 1.5 mmol, 200 mg, 0.27 mL) and 2-(2-nitroimidazolyl)ethylamine hydrochloride (1.1 mmol, 182 mg) were added to a stirred solution of TRAP (0.2 mmol, 150 mg) in dimethylsulfoxide (DMSO, 8 mL). 2-(1H-benzotriazol-1-yl)-1,1,3,3-tetramethyluronium hexafluoro phosphate (HBTU, 1.3 mmol, 500 mg) was added in small portions within 10 min. The mixture was left to react overnight at room temperature. Progress of the reaction was monitored by ESI^+-MS. The reaction mixture was injected into a preparative HPLC (0–45% of B with A for 40 min) for purification. The peaks containing the desired products (R_t = 21.4 min, **5**; R_t = 19.6 min, **4**) were collected and the solutions were evaporated to dryness under reduced pressure. Recrystallization in isopropanol gave pure compounds **4** (38 mg, 30.8%) and **5** (43 mg, 29.2%) as pale yellow solids. After purification, the products were injected into an analytical HPLC under the same conditions used for purification, and single peaks were observed for both products. **4:** ^{1}H NMR (D_2O): δ 7.43 (s, 1H), 7.19 (s, 1H), 4.61–4.59 (t, 2H, J = 5.28 Hz), 3.70–3.68 (t, 2H, J = 5.28 Hz), 3.51–3.49 (m, 12H), 3.44–3.43 (d, 4H, J = 5.66 Hz), 3.36–3.35 (d, 2H, J = 5.66 Hz), 2.69–2.64 (m, 4H), 2.42–2.37 (m, 2H), 2.06–2.02 (m, 4H), 1.90–1.86 (m, 2H); ^{13}C NMR (D_2O) δ 180.37, 178.55, 147.53, 131.54, 130.71, 57.91, 57.31, 54.50, 54.40, 54.20, 44.05, 41.69, 30.70, 29.72, 28.40, 27.77, 23.21; ^{31}P NMR (D_2O) δ 39.30, 38.74. HRMS (ESI^+), $(M + H)^+$calcd for $C_{23}H_{42}N_7O_{13}P_3$, 718.2123; found, 718.2128. **5:** ^{1}H NMR (D_2O) δ

7.43 (s, 2H), 7.19 (s, 2H), 4.61–4.59 (t, 4H, J = 5.66 Hz), 3.70–3.68 (t, 4H, J = 5.66 Hz), 3.48–3.46 (m, 12H), 3.42–3.41 (d, 2H, J = 6.04 Hz), 3.34–3.33 (d, 4H, J = 5.66 Hz), 2.69–2.64 (m, 2H), 2.42–2.37 (m, 4H), 2.06–2.37(m, 2H), 1.90–1.85 (m, 4H); ^{13}C NMR (D_2O) δ 178.06, 147.49, 131.50, 130.66, 57.30, 54.49, 54.32, 54.17, 52.35, 41.66, 30.65, 29.72, 28.92, 28.30, 26.62; ^{31}P NMR (D_2O) δ 39.28, 38.68. HRMS (ESI^+), $(M + H)^+$calcd for $C_{28}H_{48}N_{11}O_{14}P_3$, 856.2670; found, 856.2670.

2-2-2. 1,4,7-triazonane-1,4,7-triyl(tris(methylene)tris(3-(2-(2-nitroimidazolyl) ethylamino)-3-oxopropylphosphinic acid (6).

DIPEA (1.2 mmol, 178 mg, 0.24 mL) and 2-(2-nitroimidazolyl)ethylamine hydrochloride (1.0 mmol, 162 mg) were added to a stirred solution of **3** (0.1 mmol, 100 mg) in DMSO (2 mL). HBTU (1.2 mmol, 460 mg) was added in small portions within 10 min. The mixture was left to react overnight at room temperature. The reaction progress was monitored by ESI^+-MS. The reaction mixture was injected into a preparative HPLC (0–45% of B with A for 40 min) for purification. The peak containing the desired product was collected at R_t = 22.9 min and the solution was evaporated to dryness under reduced pressure. Recrystallization in isopropanol gave pure compound **6** as a pale yellow solid (62 mg, 36.2%). After purification, the product obtained was injected into an analytical HPLC under the same conditions used for purification, and a single

peak was observed. ^{1}H NMR (D_2O) δ 7.43 (s, 3H), 7.18 (s, 3H), 4.61–4.59 (t, 6H, J = 5 .66 Hz), 3.69–3.67 (t, 6H, J = 5.66 Hz), 3.44 (s, 12H), 3.329–3.320 (d, 6H, J = 5.66 Hz), 2.41–2.37 (m, 6H), 1.89–1.84 (m, 6H); ^{13}C NMR (D_2O) δ 178.07, 147.47, 131.49. 130.66, 57.33, 56.75, 54.33, 52.34, 41.65, 30.69, 28.91, 28.29, 26.61; ^{31}P NMR (D_2O) δ 39.13. HRMS (ESI^+), $(M + H)^+$calcd for $C_{33}H_{54}N_{15}O_{15}P_3$, 994.3215; found, 994.3216.

2-2-3. $^{nat}Ga^{III}$ complexes of TRAP (3) derivatives.

Each 1 mmol/0.5 mL (pH 3.0) aqueous solution of the TRAP derivative and $Ga(NO_3)_3$ was mixed in a 5-mL vial and heated at 95 °C for 10 min in a water bath. Formation of the Ga^{III} complex was confirmed by mass spectrometry [58]. $^{nat}Ga^{III}$ complexed-nitroimidazole derivatives were purified by HPLC.

^{nat}Ga-**4:** Mass spectrum (ESI+), $(M)^+$ calcd. for $C_{23}H_{39}GaN_7O_{13}P_3$, 784.23; found, 784.

^{nat}Ga-**5:** Mass spectrum (ESI+), $(M)^+$ calcd. for $C_{28}H_{45}GaN_{11}O_{14}P_3$, 922.36; found, 922.

^{nat}Ga-**6:** Mass spectrum (ESI+), $(M)^+$ calcd. for $C_{33}H_{51}GaN_{15}O_{15}P_3$, 1060.49; found, 1060.

2-3. Radiolabeling

$^{68}GaCl_3$ (0.2 mL, 199 MBq) eluted from a ^{68}Ge/^{68}Ga-generator using 0.05

M HCl was added to a solution of **3** (10 nmol) in NaOAc buffer (1 M, pH 4.5, 0.2 mL), and then the mixture was heated in a 95 °C aluminum block for 10 min. The labeled derivatives were passed through an alumina-N cartridge pre-washed with water and monitored by ITLC-SG using 0.1 M Na_2CO_3 solution as a mobile phase to verify labeling efficiency (Supporting Information Figure S1). Ten nmol of each **4**, **5**, and **6** was labeled with ^{68}Ga (82–199 MBq) using the same procedure. Then the labeled compounds (^{68}Ga-**4**, ^{68}Ga-**5** and ^{68}Ga-**6**) radiochemical purities were measured by radio-HPLC.

2-4. Stability study

The ^{68}Ga-**3**, ^{68}Ga-**4**, ^{68}Ga-**5**, and ^{68}Ga-**6** were stored in prepared medium at room temperature and in human serum at 37 °C for 10, 30, 60, 120, and 240 min and then analyzed using ITLC-SG/0.1 M Na_2CO_3 (the $^{68}Ga^{3+}$ remained at the origin and the labeled products moved with the solvent front) and 0.1 M citric acid (the $^{68}Ga^{3+}$ moved with the solvent front and the labeled products remained at the origin) was used as the mobile phase.

2-5. Measurement of partition coefficients

Na_2HPO_4 buffer (0.1 M, pH 7.4, 2 g) was added to octanol (2 g), and then ^{68}Ga-**3** (0.37 MBq/2 μL) was added, mixed vigorously, and centrifuged (3,000 rpm for 5 min). The radioactivities of the octanol fraction (0.5 g) and the 0.1

M Na_2HPO_4 buffer fraction (0.5 g) were measured using a γ scintillation counter, and log P values were calculated. The same procedure was used for ^{68}Ga-**4**, ^{68}Ga-**5,** and ^{68}Ga-**6**.

2-6. Measurement of serum protein binding

Human serum protein binding assays were performed as previously described [61, 62]. PD-10 columns were preconditioned by loading 1.0 mL of 1% bovine serum albumin in 0.1 M diethylenetriaminepentaacetic acid (DTPA) and eluted with 100 mL of phosphate buffered saline (PBS). ^{68}Ga-**3** (1.1 MBq/10 μL) was mixed with human serum (1 mL) and incubated for 60 min at 37 °C. Each mixture was loaded onto a preconditioned PD-10 column and eluted with PBS; 30 fractions (fraction size = 0.5 mL) were collected per sample in 5-mL test tubes. The radioactivity of each fraction was measured using a γ-scintillation counter and expressed as cpm (counts per minute). To verify the presence of protein in each fraction, an aliquot (2 μL) from each test tube was spotted on a filter paper and stained with Coomassie blue. Percentage protein bindings were calculated using fraction activity curves. The same procedure was used for the other labeled agents.

2-7. *In vitro* cellular uptake study

Cellular uptake studies were performed using the U87MG and CT-26 cell

lines. The U87MG cell line was maintained in minimum essential medium (MEM) and the CT-26 cell line was maintained in Dulbecco's modified Eagle's medium (DMEM), both media obtained from Welgene Inc., Korea. Both media were maintained (10% fetal bovine serum and a 1% mixture of antibiotics (penicillin:streptomycin:amphotericin B = 10,000 IU:10 mg:25 μg in 1 mL, Mediatech Inc., Manassas, VA, U.S.A.)) in an incubator with 5% CO_2 atmosphere and at 37°C. The cells were subcultured overnight in 24-well plates (2×10^5 cells/well). Preincubation was performed under normoxic (5% CO_2 in air) or hypoxic (5% CO_2 in 95% N_2) conditions for 4 h. ^{68}Ga-**3** (0.18 MBq/100 μL) was added to each well and incubated for 15, 30, and 60 min. Wells were washed twice with 1 mL DMEM and the cells were dissolved in 0.5% sodium dodecyl sulfate (SDS) in 0.1 mL PBS. Tracer uptake was measured using a γ-scintillation counter and the total protein concentrations of samples were determined using the bicinchoninic acid method (Pierce, Rockford, IL, U.S.A.). The same procedure was used for the other labeled agents.

2-8. Immunohistochemical analysis

Hypoxyprobe™-1 (pimonidazole hydrochloride (60 mg/kg)) was diluted in 150 μL of PBS and intravenously injected into each CT-26 xenografted mouse (n = 3). Mice were sacrificed at 1.5 h post-injection. The tumor was

isolated and directly frozen in liquid nitrogen until cryosectioning into 7-µm thin slices using a Leica CM1800 Cryostat (IMEB Inc., CA, U.S.A.). The sections were then stored at -80°C until staining. The fixed tumor sections were washed with PBS containing 0.2% Brij 35 and exposed to 3% hydrogen peroxide for 5 min at room temperature to quench endogenous peroxidase activity. The sections were incubated with a protein-blocking agent for 5 min at room temperature to minimize nonspecific binding. The samples were incubated for 60 min at room temperature with mouse monoclonal anti-pimonidazole antibody (MAb1) diluted in PBS, and washed. Samples were incubated with a secondary biotinylated antibody (Vector Laboratories Inc., Burlingame, CA, U.S.A.) and with a biotin-streptavidin-peroxidase complex, and, finally, with 3,3′-diaminobenzidine (DAB), which imparts a clear brown color to the marker-antibody complex around the nucleus of the hypoxic cells. Between all steps of the staining procedure, the sections were rinsed three times with PBS (0.2% Brij 35) for 2 min at 0°C. Finally, the sections were mounted with CC/Mount from Sigma/Aldrich (St. Louis, MO, U.S.A.). The cells and histological sections were viewed with a microscope (Olympus America Inc., Melville, NY, U.S.A.) to investigate whether they were stained brown, indicating hypoxia.

2-9. Biodistribution study of xenografted mice

CT-26 cells cultured in DMEM containing 10% fetal bovine serum were harvested after treatment with 0.05% trypsin. Cells were washed with 10 mL of PBS by centrifugation (3000 rpm). Each BALB/c mouse was subcutaneously injected with 2×10^5/0.1 mL CT-26 cells in the right shoulder. After 2 weeks, ^{68}Ga-labeled agents (0.37 MBq/0.1 mL) were intravenously injected into each xenografted mouse (n = 4). Mice were sacrificed at 1 h post-injection. Tumor, blood, muscle, and other organs were separated immediately, and their weights and radioactivity values were obtained using a balance and a γ-scintillation counter, respectively. Results are expressed as the percentage of injected dose per gram of tissue (% ID/g). The same procedure was used for the other labeled agents**.**

2-10. PET of tumor-bearing mice

CT-26 cells (2×10^5 cells) in normal saline (0.1 mL) were subcutaneously injected into the right shoulders of the mice and grown for 14 days to produce tumors of ~16 mm in diameter. ^{68}Ga-**3** (23 MBq/0.1 mL) was intravenously injected through the tail vein (n=3). Mice were anesthetized with 2% isoflurane by inhalation and PET images were obtained at 1 h. PET studies were performed using a dedicated small-animal PET scanner. Emission data were acquired for 20 min. The three-dimensional raw emissions data were

reconstructed to temporally framed sinograms by Fourier rebinning, using an ordered subset expectation maximization (OS-EM) reconstruction algorithm attenuation correction. For the PET images, data from 20 frames were analyzed (10 times with 1-min frames). The same procedure was used for the other labeled agents.

2-11. Data analysis

The software AsiPro VM 5.0 from Concorde Inc., (Knoxville, TN, U.S.A.) was used to process images. To assess uptake of the labeled derivatives by tumors cells, circular regions of interests (ROI) were placed (1.5-mm radius) at locations of maximum tracer uptake in tumors and in muscles as references. Relative tracer uptake was expressed as the ratio of tumor to muscle counts. Having placed ROIs, standard uptake values (SUVs) were calculated using the equation SUV = CCF/(injected dose/body weight of mouse). The CCF (decay-corrected activity concentration) was calculated using the equation CCF (MBq/mL) = radioactivity (mCi/mL) × branching ratio × ROI (value/pixel); the branching ratio of ^{68}Ga is 0.891.

3. Results and Discussions

3-1. Synthesis

TRAP (**3**) was synthesized according the previously reported methods [48]. Compared to the other ligands, synthesis of TRAP is more simple, fast and scalable. Moreover, protection is not required before conjugation with ligands by amide formation [48, 58]. The nitroimidazole residue, 2-(2-nitroimidazolyl)ethylamine hydrochloride was also synthesized according to a previously published method [53, 54].

The nitroimidazole residue, 2-(2-nitroimidazolyl)ethylamine was conjugated with **3** via an acid-amine coupling reaction in dimethylsulfoxide (DMSO) using 2-(1H-benzotriazol-1-yl)-1,1,3,3-tetramethyluronium hexafluorophosphate (HBTU) as a coupling agent in the presence of *N,N*-diisopropylethylamine (DIPEA) as a base (Scheme 1). The yields of the prepared derivatives **4**, **5**, and **6** were 30.8%, 29.2%, and 36.2%, respectively. The chemical structures of the final products were confirmed by NMR and ESI^+-MS. Their purities were verified by analytical HPLC, and were confirmed by appearance of single peaks.

Complexes of natural gallium with the synthesized compounds were obtained by reaction with $Ga(NO_3)_3$ in aqueous solution [58]. Product formation of the Ga^{III} complex was confirmed by MS-ESI^+.

3-2. Radiochemistry

Radiolabeling with ^{68}Ga was conducted at pH 4.5 at 95 °C in an aluminum heating block for 10 min. Labeling efficiencies of the prepared derivatives were verified by ITLC using 0.1 M Na_2CO_3 (the $^{68}Ga^{3+}$ remained at the origin and the labeled products moved with the solvent front) as a mobile phase (Figure 2-3). Radiochemical yields of the prepared derivatives were found to be greater than 96% for all derivatives (Table 1). Radiochemical purities of the ^{68}Ga labeled conjugates were measured by radio-HPLC, and found to be greater than 99%. The ^{68}Ga-labeled derivatives showed low partition coefficients (log P), indicating that all are very hydrophilic (Table 1). The log P values for ^{68}Ga-**3** and ^{68}Ga-**4** could not be determined because only background radioactivity was detected in the octanol phase. Three carboxylic residues of ^{68}Ga-**3** and two carboxylic residues of ^{68}Ga-**4** might contribute high hydrophilicity. The prepared derivatives ^{68}Ga-**5** and ^{68}Ga-**6** showed lower partition coefficients (log P) values than the standard hypoxia imaging agents like [^{18}F]FMISO (2.6), [^{18}F]FAZA (1.1) [4, 63]. All of the ^{68}Ga-labeled derivatives showed lower protein-binding values (Table 1) than the reported agents such as ^{68}Ga-NOTA-SCN-NI (2.45 ± 0.06), ^{68}Ga-DOTA-NI (15.29 ± 0.28), and ^{68}Ga-DOTA-SCN-NI (14.04 ± 0.49) at 60 min time point [53, 54], which might favor rapid uptake by target tissues and rapid clearance from blood and non-target tissues. Furthermore, all showed high in vitro stability,

up to 4 h in prepared media at room temperature and in human serum at 37 °C (Figure 2-4). These stability test results show the suitability of the labeled derivatives for radiopharmaceutical applications.

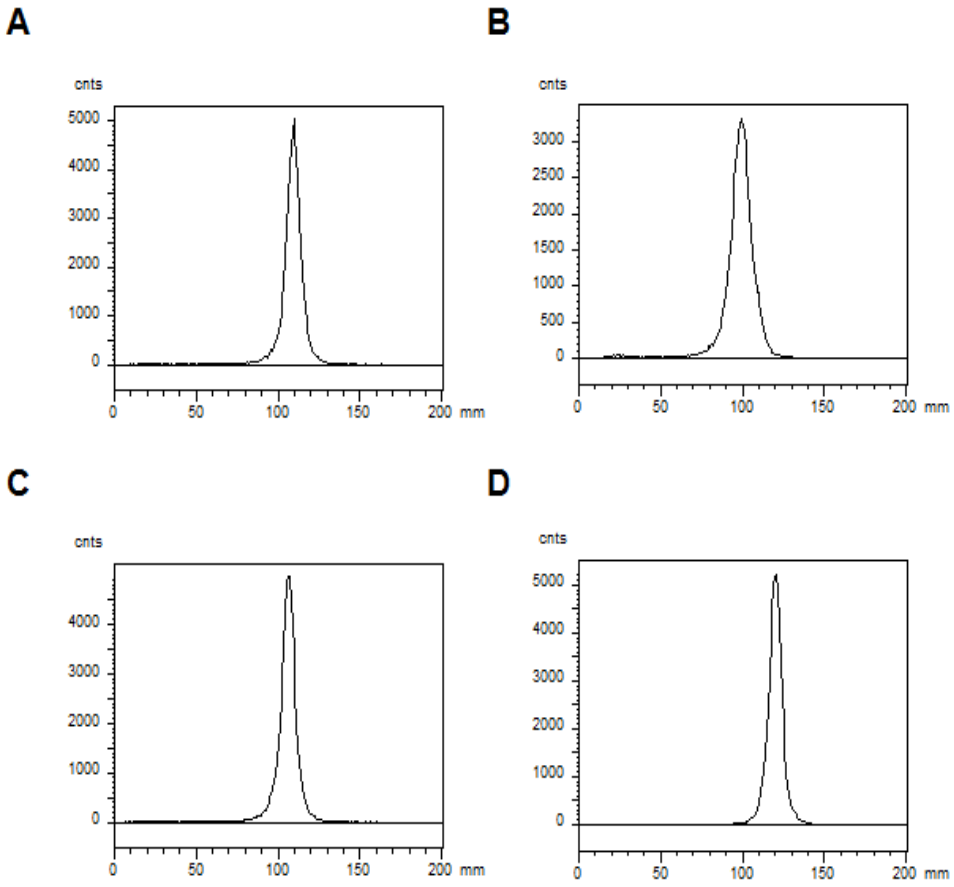

Figure 7. Radio TLC (ITLC-SG) of (A) ^{68}Ga-**3**; (B) ^{68}Ga-**4**; (C) ^{68}Ga-**5** and (D) ^{68}Ga-**6** 0.1 M Na_2CO_3 solution as a mobile phase.

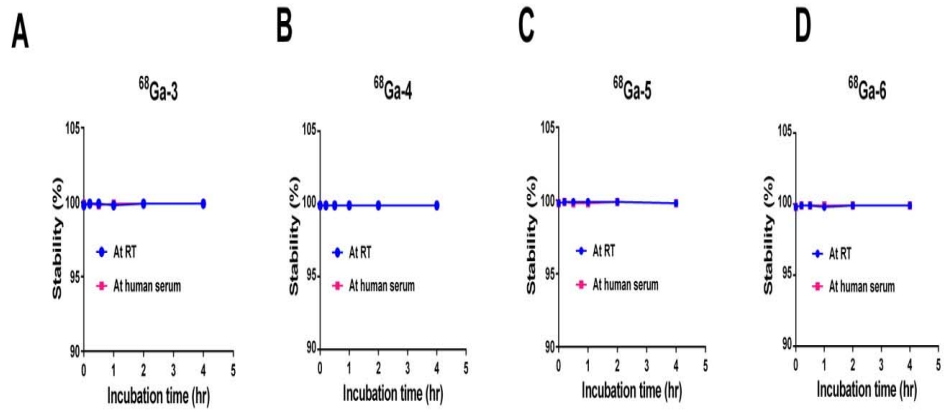

Figure 8. Stability studies of (A) ^{68}Ga-**3,** (B) ^{68}Ga-**4,** (C) ^{68}Ga-**5,** and (D) ^{68}Ga-**6** in prepared medium and in human serum.

Table 1. Partition Coefficient, Protein Binding, Radiochemical Yield, and Specific Activity of the Labeled Compounds[a]

Compound	Partition coefficient (log P)	Protein binding (%)	Radiochemical yield (%)	Specific activity (10^6 Ci/mol)
^{68}Ga-**3**	ND [b]	0.32 ± 0.02	97.9 ± 1.62	0.229 ± 0.103
^{68}Ga-**4**	ND [b]	1.18 ± 0.64	96.9 ± 2.00	0.322 ± 0.095
^{68}Ga-**5**	-3.64 ± 0.15	1.24 ± 0.12	97.4 ± 1.56	0.262 ± 0.050
^{68}Ga-**6**	-3.28 ± 0.22	1.42 ± 0.36	97.6 ± 1.28	0.291 ± 0.071

[a] The values represents mean ± SD (n = 4).

[b] No radioactivity was measured in the octanol phase.

3-3. *In vitro* cellular uptake study

U87MG (human glioblastoma) and CT-26 (mouse colon cancer) cell lines were used for the cellular uptake study. *In vitro* experiments proved that the ^{68}Ga-**6** demonstrated the most significantly increased hypoxic tumor cellular uptake, followed by ^{68}Ga-**5** under hypoxic conditions for both cell lines (Figure 2-5). The hypoxic-to-normoxic uptake ratios of ^{68}Ga-**6** in U87MG cells were 7.5, 8.2, and 6.0 at 15, 30, and 60 min, respectively; in CT-26 cells they were 5.5, 7.6, and 2.5 at 15, 30, and 60 min, respectively. The uptake ratios for ^{68}Ga-**5** in U87MG cells were 3.0, 2.3, and 1.6 at 15, 30, and 60 min, respectively; in CT-26 cells they were 1.0, 1.5, and 3.0 at 15, 30, and 60 min, respectively. The uptake ratios for ^{68}Ga-**4** in U87MG cells were 1.2, 1.1, and 1.4 at 15, 30, and 60 min, respectively; in CT-26 cells they were 2.0, 1.0, and 2.0 at 15, 30, and 60 min, respectively. For ^{68}Ga-**3**, the uptake ratios in U87MG cells were 0.5, 1.6, and 1.6 at 15, 30, and 60 min, respectively; in CT-26 cells they were 1.2, 1.5, and 1.0 at 15, 30, and 60 min, respectively. ^{68}Ga-**6** showed significantly increased ($p < 0.005$) cellular uptakes in hypoxic condition at all investigated time points, and ^{68}Ga-**5** showed significantly increased ($p < 0.05$) cellular uptake in hypoxic conditions at 60 min only. However, the other compounds did not show significantly increased cellular uptake in hypoxic conditions at any time point. This in vitro cellular uptake experiment demonstrated the increased uptake of the trivalent agent ^{68}Ga-**6** by hypoxic

cancer cells. Only ^{68}Ga-**6** showed higher hypoxic-to-normoxic uptake ratios than the reported agents such as ^{68}Ga-NOTA-NI (1.5), ^{68}Ga-NOTA-SCN-NI (2.6), ^{68}Ga-DOTA-NI (6.8), and ^{68}Ga-DOTA-SCN-NI (3.4) at 60 min time point in CT-26 cell lines [53, 54].

It has been reported that the introduction of second 2-nitroimidazole residue greatly enhanced the hypoxic accumulation in murine sarcoma S180 cells in *in-vitro* cell uptake study. An increase of 2.4 fold hypoxia cell uptake was observed in ^{99m}Tc-labelled bisnitroimidazole derivative (59.0 ± 0.9%) than the corresponding ^{99m}Tc-labelled mono-nitroimidazole (24.4 ± 3.9%) at 4 h [56].

In the present study, ^{68}Ga-**6** showed 7.7 and 8.2 fold increased cellular uptakes than ^{68}Ga-**5** and ^{68}Ga-**4**, respectively, in U87MG cell line at 60 min in hypoxic condition. ^{68}Ga-**6** showed 7.4 and 22 fold increased cellular uptakes than ^{68}Ga-**5** and ^{68}Ga-**4**, respectively, in CT-26 cell line at 60 min in hypoxic condition (Figure 3). ^{68}Ga-**5** also showed 1.0 and 3.0 fold increased cellular uptakes in U87MG and CT-26 cell lines, respectively, than ^{68}Ga-**4** at 60 min in hypoxic condition (Figure 3).

In vitro cell uptake experiment can be concluded that the uptake of the labeled agents by hypoxic cancer cells increased with positive correlation with the conjugated nitroimidazole number, and thus ^{68}Ga-**6** showed the most significantly increased uptake at all investigated time points (Figure 3).

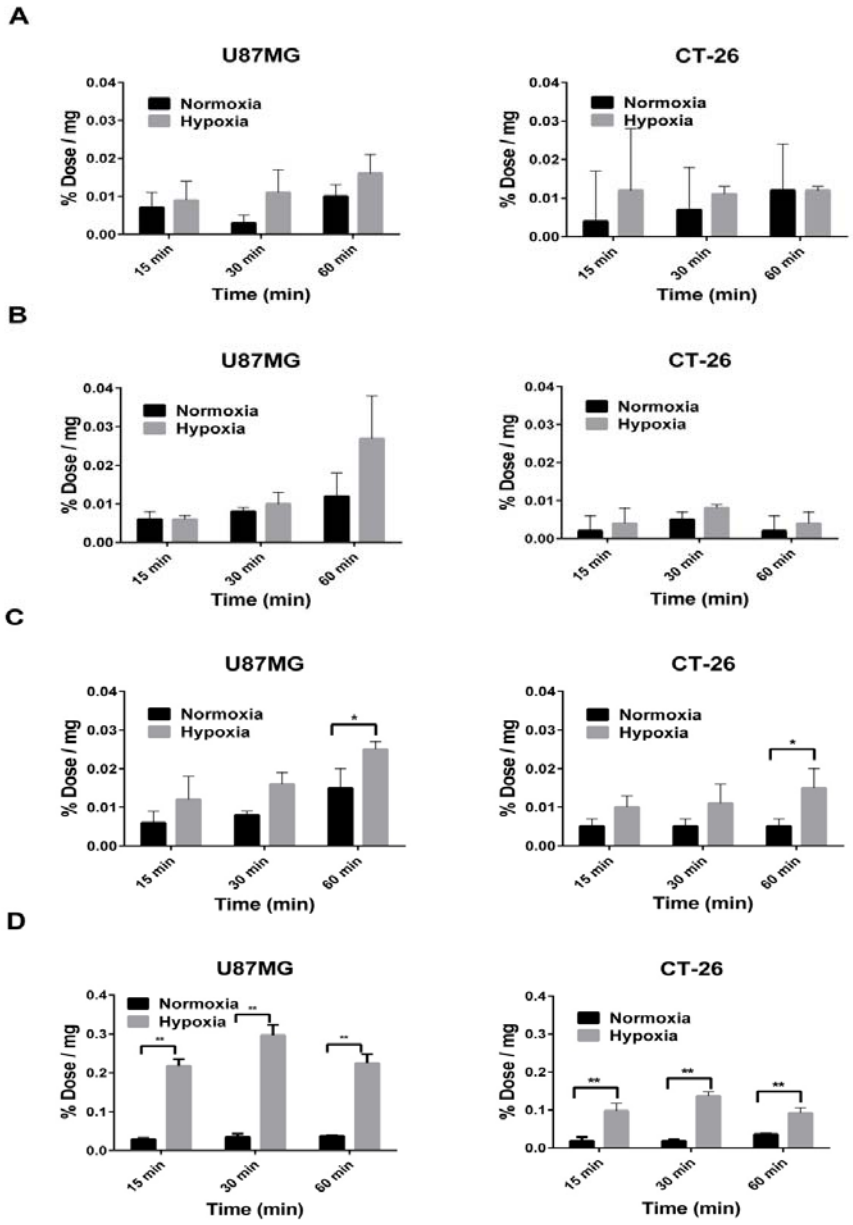

Figure 9. *In vitro* cellular uptake studies for determination of the specific uptake of the novel tracers (A) ^{68}Ga-**3,** (B) ^{68}Ga-**4,** (C) ^{68}Ga-**5,** and (D) ^{68}Ga-**6** under normoxic and hypoxic conditions using U87MG and CT-26 cells. P-values show comparisons of uptake under normoxic and hypoxic conditions (*t*-test): (**) $p < 0.005$, (*) $p < 0.05$, $n = 3$ at each time point.

3-4. Immunohistochemistry

The presence of hypoxia in the CT-26 xenografted tumor tissue was verified by immunohistochemical analysis. After injection of a standard exogenous hypoxia marker, pimonidazole hydrochloride, into CT-26 xenografted mice via the tail vein, the mice were sacrificed at 1.5 h post-injection. The tumors were dissected and cut into 7-μm slices at -20 °C, and then were processed using the antibody kit obtained from Hypoxyprobe. Immunohistochemical staining (brown) revealed the presence of hypoxic areas (Figure 2-6).

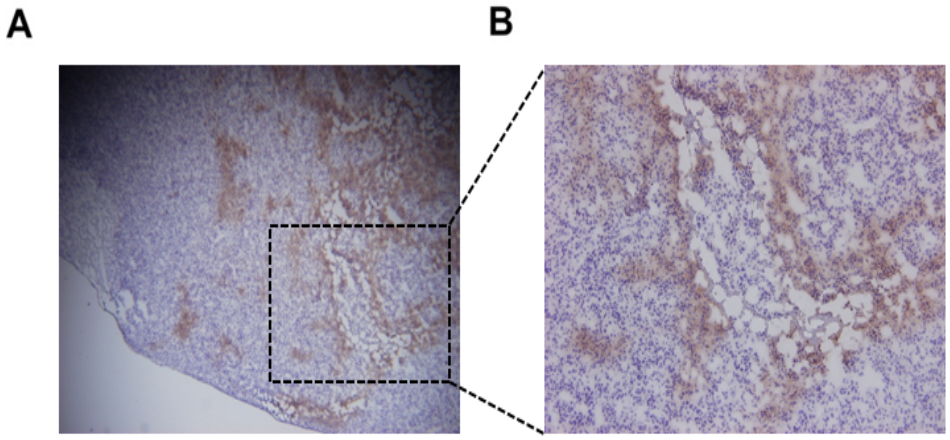

Figure 10. Immunohistochemical staining of CT26 tumor xenografts to detect hypoxia. Tumor tissue was obtained from xenografted mice at 1.5 h after intravenous injection of Hypoxyprobe^{TM}-1. Hypoxic lesions are shown in brown. (A) 40× and (B) 100× magnification images.

3-5. Biodistribution in xenografted mice

A biodistribution study was performed using mouse colon cancer CT-26 xenografted BALB/c mice after injection of ^{68}Ga-**3**, ^{68}Ga-**4**, ^{68}Ga-**5**, and ^{68}Ga-**6** (0.37 MBq/0.1 mL) via the tail vein (Table 2). Mice were sacrificed at 1 h post-injection. Among the organs evaluated, the kidneys showed the highest uptake for all the labeled agents (^{68}Ga-**3**: 1.65 ± 0.07 ^{68}Ga-**4**: 2.06 ± 0.22, ^{68}Ga-**5**: 2.64 ± 0.36, and ^{68}Ga-**6**: 2.72 ± 0.21% ID/g) indicating that the major excretion route is via kidneys. However, the nitroimidazole-conjugated derivatives did not differ significantly in kidney uptake. The prepared derivatives in the present study showed improved clearance properties than [^{18}F]fluoromisonidazole ([^{18}F]FMISO), demonstrating that kidney is the major excretion pathway for the prepared derivatives in this study, whereas [^{18}F]FMISO clearance mainly occurs through the hepatobiliary and gastrointestinal pathway [21].

At 1 h post-injection, the liver uptake of the labeled agents ^{68}Ga-**3,** ^{68}Ga-**4,** ^{68}Ga-**5,** and ^{68}Ga-**6** was 0.15 ± 0.01, 0.24 ± 0.05, 0.29 ± 0.02, and 0.34 ± 0.06% ID/g, respectively. The results demonstrated that the liver uptake increased by hydrophobicity.

Table 2. Biodistribution of ^{68}Ga-Labeled Derivatives in CT-26 Xenografted Mice after 1 h Post-injection[a]

Organ	^{68}Ga-**3**	^{68}Ga-**4**	^{68}Ga-**5**	^{68}Ga-**6**
Blood	0.22 ± 0.04	0.41 ± 0.09	0.54 ± 0.04	0.52 ± 0.16
Muscle	0.12 ± 0.02	0.17 ± 0.02	0.21 ± 0.01	0.20 ± 0.14
Tumor	0.17 ± 0.04	0.33 ± 0.04	0.45 ± 0.09	0.47 ± 0.05
Heart	0.07 ± 0.02	0.16 ± 0.06	0.19 ± 0.04	0.24 ± 0.09
Lung	0.22 ± 0.04	0.38 ± 0.07	0.60 ± 0.05	0.75 ± 0.14
Liver	0.15 ± 0.01	0.24 ± 0.05	0.29 ± 0.02	0.34 ± 0.06
Spleen	0.09 ± 0.02	0.17 ± 0.03	0.19 ± 0.03	0.29 ± 0.06
Stomach	0.09 ± 0.02	0.22 ± 0.12	0.26 ± 0.04	0.32 ± 0.08
Intestine	0.15 ± 0.05	0.24 ± 0.07	0.38 ± 0.02	0.50 ± 0.06
Kidney	1.65 ± 0.07	2.06 ± 0.22	2.64 ± 0.36	2.72 ± 0.21

[a] Data are expressed as mean ± SD% ID/g (n = 4).

The uptake of the labeled agents by tumor was positively correlated with the conjugated nitroimidazole number (^{68}Ga-**3**: 0.17 ± 0.04, ^{68}Ga-**4**: 0.33 ± 0.04, ^{68}Ga-**5**: 0.45 ± 0.09, and ^{68}Ga-**6**: 0.47 ± 0.05% ID/g). All ^{68}Ga-nitroimidazole derivatives in this study showed significantly higher uptake by tumor cells than the control agent ^{68}Ga-**3** ($p < 0.05$) at 1 h post-injection (Table 2). Furthermore, ^{68}Ga-**6** also showed significantly higher uptake by tumor cells than ^{68}Ga-**4** at 1 h post-injection ($p < 0.05$). At 1 h post-injection, the relative tumor retention rates were ^{68}Ga-**4** < ^{68}Ga-**5** < ^{68}Ga-**6**, indicating a multi-valent effect.

All ^{68}Ga-nitroimidazole derivatives in this study showed higher tumor-to-blood uptake ratios (^{68}Ga-**3**: 0.78 ± 0.13, ^{68}Ga-**4**: 0.80 ± 0.23, ^{68}Ga-**5**: 0.84 ± 0.15, and ^{68}Ga-**6**: 0.89 ± 0.12) than ^{68}Ga-NOTA-NI (0.62), ^{68}Ga-NOTA-SCN-NI (0.73), ^{68}Ga-DOTA-NI (0.73), and ^{68}Ga-DOTA-SCN-NI (0.65) at 1 h post-injection [22, 23]. Tumor-to-muscle uptake ratios of the of the labeled agents ^{68}Ga-**3**, ^{68}Ga-**4**, ^{68}Ga-**5**, and ^{68}Ga-**6** were, 1.41 ± 0.33, 1.94 ± 0.12, 2.14 ± 0.19, and 2.35 ± 0.17, respectively. Only ^{68}Ga-**6** also showed a higher tumor-to-muscle ratio than the reported agents ^{68}Ga-NOTA-NI (2.13) and ^{68}Ga-NOTA-SCN-NI (1.64) at 1 h post-injection [53, 54].

Thus, of the three agents tested, ^{68}Ga-**6** showed the highest mean tumor uptake, tumor-to-blood and tumor-to-muscle ratios at 1 h post-injection. The blood activity was always higher than tumor uptake due to the lower blood

flow in the hypoxic than in the normoxic tumor, which is common finding of hypoxia imaging. However, ^{68}Ga-**6** has own advantage over the currently available ^{18}F-labeled nitroimidazole derivatives. Because ^{68}Ga can be obtained from a generator which is much more economical and convenient than a cyclotron.

3-6. PET imaging of tumor bearing mice.

A small animal PET study was performed using CT-26 xenografted mice. Images were obtained at 1 h after intravenous injection of ^{68}Ga-**3**, ^{68}Ga-**4**, ^{68}Ga-**5**, and ^{68}Ga-**6** (23 MBq/ 0.1 mL) into the mice via the tail vein (Figure 2-7). All agents showed high rates of kidney and bladder uptake, as predicted from the biodistribution study. ^{68}Ga-**6** demonstrated higher uptake by tumor tissues than the other labeled agents. Standardized uptake values (SUVs) were calculated, using the PET images. ^{68}Ga-**6** showed a higher SUV than the other labeled agents (^{68}Ga-**3**: 0.10 ± 0.06; ^{68}Ga-**4**: 0.20 ± 0.06; ^{68}Ga-**5**: 0.33 ± 0.08; ^{68}Ga-**6**: 0.59 ± 0.09) at 1 h post-injection. ^{68}Ga-**6** also showed a higher mean SUV than the reported agents ^{68}Ga-NOTA-NI (0.30 ± 0.2), ^{68}Ga-NOTA-SCN-NI (0.19 ± 0.1), ^{68}Ga-DOTA-NI (0.53 ± 0.1), and ^{68}Ga-DOTA-SCN-NI (0.17 ± 0.1) at 1 h post-injection [22, 23]. Moreover, tumor-to-non-tumor SUV ratio of ^{68}Ga-**6 (**7.41 ± 1.12) was higher than ^{68}Ga-**3** (2.97 ± 0.01), ^{68}Ga-**4** (3.50 ± 0.02), and ^{68}Ga-**5** (4.12 ± 0.06). ^{68}Ga-**6** also showed a higher tumor-to-muscle

SUV ratios than the reported agents ^{68}Ga-NOTA-NI (5.70 ± 2.5), ^{68}Ga-NOTA-SCN-NI (3.95 ± 1.3), ^{68}Ga-DOTA-NI (5.64 ± 0.8), and ^{68}Ga-DOTA-SCN-NI (3.83 ± 0.8) at 1 h post-injection [53, 54].

Although the level of uptake in the kidneys was high, it is acceptable for a PET agent because it can be easily kept under a hazardous radiation level and would seldom disturb image reading or analysis [36]. The trivalent derivative ^{68}Ga-**6** also showed the highest SUV for tumor tissues at 1 h post-injection, which is consistent with in vitro experiment (Figure 4).

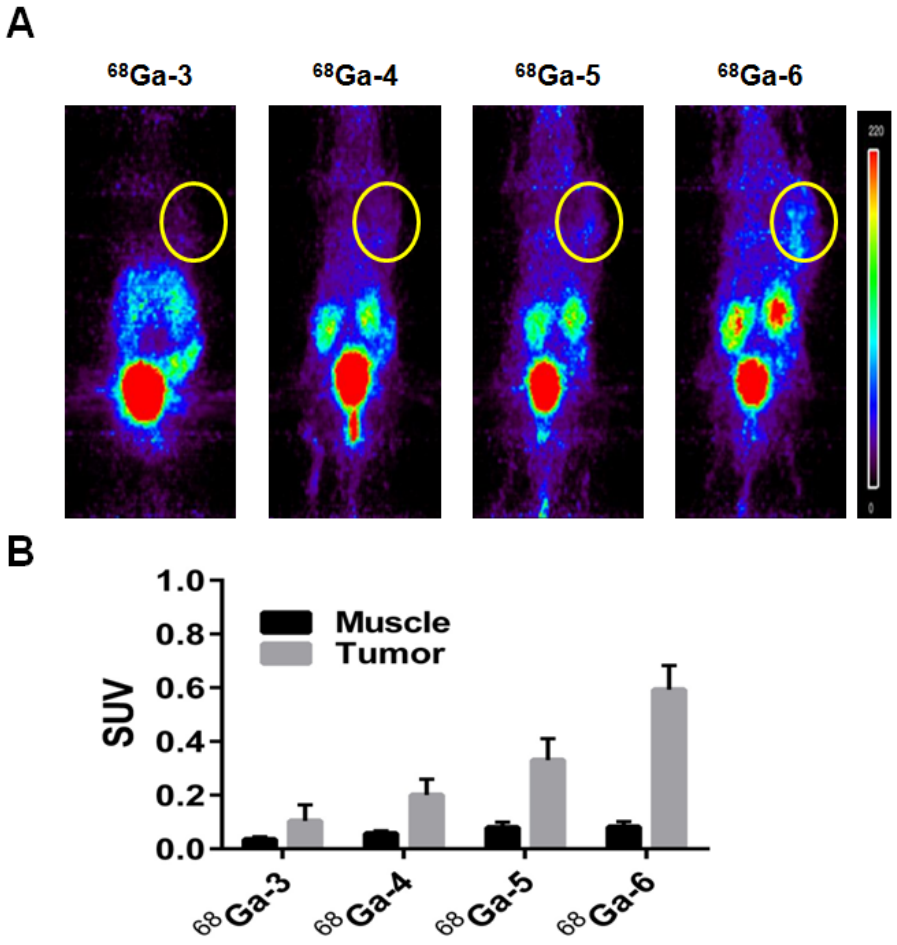

Figure 11. Small animal PET images of ^{68}Ga-labeled nitroimidazole derivatives. Images of mice bearing colon cancer CT-26 xenografts were recorded at (A) 1 h post-injection (23 MBq/0.1 ml per mouse via the tail vein). SUVs obtained after (B) 1 h and post-injection from animal PET images.

The clinical importance of hypoxia PET imaging using various agents such as [^{18}F]fluoromisonidazole ([^{18}F]FMISO), [^{18}F]fluoroazomycin ([^{18}F]FAZA), 3-[^{18}F]fluoro-2-(4-((2-nitro-1H-imidazol-1-yl)methyl)-1H-1,2,3-triazol-1-yl)propan-1-ol ([^{18}F]HX4), [^{18}F]fluoroerythronitroimidazole ([^{18}F]FETNIM), and [^{64}Cu] diacetyl-bis(N4-methylthiosemicarbazone ([^{64}Cu]-ATSM) have been reviewed [64]. A large heterogeneity in uptake, imaging time, and tumor and animal models for different hypoxia markers have been observed in the literature, making comparison hard to interpret [21]. The above mentioned nitroimidazole derivatives have been developed to overcome some of the limitations of [^{18}F]FMISO such as nonspecific retention, metabolic conversion, and low partition coefficient, all leading to faster clearance properties [65]. Radioresistant hypoxic lesions of various cancers including glioma, head and neck cancer, brain tumor, pancreatic cancer, uterine cervix cancer, and rectal cancer have been imaged using the above agents, and concluded that the development of improved agent would make PET imaging and hypoxic modification a standard of care in the clinical setting for many cancer types. We hope that ^{68}Ga-**6** could be one of the such new agents.

4. Conclusion

We synthesized derivatives of the chelating agent TRAP (**3**) conjugated with one, two, and three nitroimidazole residues **4**, **5**, and **6**, respectively. All derivatives, including **3** as a control, were labeled with ^{68}Ga; all conjugates were labeled with high efficiency (>99%). The labeled agents were stable in prepared medium at room temperature and in human serum at 37°C. In vitro cell uptake experiments using U87MG and CT-26 cell lines showed that a trisnitroimidazole derivative, ^{68}Ga-**6**, lead to significant increase in the hypoxic to normoxic uptake ratio**.** Immunohistochemical staining of tumor hypoxia using Hypoxyprobe^{TM}-1 showed the presence of hypoxia lesions in CT-26 tumor xenograft tissue. A biodistribution study in CT-26 xenografted mice showed that the increased tumor-to-muscle ratios and were rapidly cleared from the blood and other non-target tissues. ^{68}Ga-**6** showed higher uptake by tumor tissues than the other labeled agents. In the PET study, ^{68}Ga-**6** also showed the highest SUV at 1 h post-injection. Although the hypoxic tumor uptake was not very high due to low blood flow, ^{68}Ga-**6**, which has an advantages over ^{18}F-labeled agents in practicability, showed an excellent image compare to the other agents. In conclusion, we successfully developed a novel trivalent ^{68}Ga-labeled nitroimidazole derivative for hypoxic tissue imaging.

5. References

1. Nunn A, Linder K, Strauss HW. Nitroimidazoles and imaging hypoxia. *Eur. J. Nucl. Med*. 1995;22(3):265-80.
2. Rauth A, Melo T, Misra V. Bioreductive therapies: an overview of drugs and their mechanisms of action. *Int. J. Radiat. Oncol. Biol. Phys*. 1998;42(4):755-62.
3. Takasawa M, Moustafa RR, Baron J-C. Applications of nitroimidazole in vivo hypoxia imaging in ischemic stroke. *Stroke*. 2008;39(5):1629-37.
4. Sorger D, Patt M, Kumar P, Wiebe LI, Barthel H, Seese A, et al. [^{18}F] Fluoroazomycinarabinofuranoside (^{18}FAZA) and [^{18}F] Fluoromisonidazole (^{18}FMISO): a comparative study of their selective uptake in hypoxic cells and PET imaging in experimental rat tumors. *Nucl Med Biol*. 2003;30(3):317-26.
5. Kizaka-Kondoh S, Konse-Nagasawa H. Significance of nitroimidazole compounds and hypoxia-inducible factor-1 for imaging tumor hypoxia. *Cancer Sci.* 2009;100(8):1366-73.
6. Fujibayashi Y, Taniuchi H, Yonekura Y, Ohtani H, Konishi J, Yokoyama A. Copper-62-ATSM: A new hypoxia imaging agent with

high membrane permeability and low redox potential. *J Nucl Med*. 1997;38(7):1155-60..

7. Martin GV, Caldwell JH, Rasey JS, Grunbaum Z, Cerqueira M, Krohn KA. Enhanced binding of the hypoxic cell marker [3H]fluoromisonidazole in ischemic myocardium. *J Nucl Med*. 1989;30(2):194-201.

8. Rajendran JG, Schwartz DL, O'Sullivan J, Peterson LM, Ng P, Scharnhorst J, et al. Tumor hypoxia imaging with [F-18] fluoromisonidazole positron emission tomography in head and neck cancer. *Clin. Ca. Res*. 2006;12(18):5435-41.

9. Lee ST, Scott AM. Hypoxia positron emission tomography imaging with ^{18}F-fluoromisonidazole. *Semin Nucl Med.* 2007;37(6):451-61.

10. Grosu A-L, Souvatzoglou M, Röper B, Dobritz M, Wiedenmann N, Jacob V, et al. Hypoxia Imaging With FAZA-PET and Theoretical Considerations With Regard to Dose Painting for Individualization of Radiotherapy in Patients With Head and Neck Cancer. *Int. J. Radiat. Oncol. Biol. Phys*. 2007;69(2):541-51.

11. Postema EJ, McEwan AJ, Riauka TA, Kumar P, Richmond DA, Abrams DN, et al. Initial results of hypoxia imaging using 1-alpha-D: -(5-deoxy-5-[^{18}F]-fluoroarabinofuranosyl)-2-nitroimidazole (^{18}F-FAZA). *Eur J Nucl Med Mol Imaging.* 2009;36(10):1565-73.

12. Souvatzoglou M, Grosu AL, Roper B, Krause BJ, Beck R, Reischl G, et al. Tumour hypoxia imaging with [^{18}F]FAZA PET in head and neck cancer patients: a pilot study. *Eur J Nucl Med Mol Imaging.* 2007;34(10):1566-75.

13. Piert M, Machulla HJ, Picchio M, Reischl G, Ziegler S, Kumar P, et al. Hypoxia-specific tumor imaging with ^{18}F-fluoroazomycin arabinoside. *J Nucl Med*. 2005;46(1):106-13.

14. Reischl G, Dorow DS, Cullinane C, Katsifis A, Roselt P, Binns D, et al. Imaging of tumor hypoxia with [^{124}I] IAZA in comparison with [^{18}F] FMISO and [^{18}F] FAZA–first small animal PET results. *J Pharm Pharm Sci.* 2007;10(2):203-11.

15. Gronroos T, Bentzen L, Marjamaki P, Murata R, Horsman MR, Keiding S, et al. Comparison of the biodistribution of two hypoxia markers [^{18}F]FETNIM and [^{18}F]FMISO in an experimental mammary carcinoma. *Eur J Nucl Med Mol Imaging*.2004;31(4):513-20.

16. Mahy P, De Bast M, Leveque P, Gillart J, Labar D, Marchand J, et al. Preclinical validation of the hypoxia tracer 2-(2-nitroimidazol-1-yl)-N-(3, 3, 3-[^{18}F] trifluoropropyl) acetamide,[^{18}F] EF3. *Eur J Nucl Med Mol Imaging*. 2004;31(9):1263-72.

17. Ziemer LS, Evans SM, Kachur AV, Shuman AL, Cardi CA, Jenkins WT, et al. Noninvasive imaging of tumor hypoxia in rats using the 2-nitroimidazole ^{18}F-EF5. *Eur J Nucl Med Mol Imaging*. 2003;30(2):259-66.

18. Komar G, Seppanen M, Eskola O, Lindholm P, Gronroos TJ, Forsback S, et al. ^{18}F-EF5: a new PET tracer for imaging hypoxia in head and neck cancer. *J Nucl Med*. 2008;49(12):1944-51.

19. Yapp DT, Woo J, Kartono A, Sy J, Oliver T, Skov KA, et al. Non-invasive evaluation of tumour hypoxia in the Shionogi tumour model for prostate cancer with ^{18}F-EF5 and positron emission tomography. *BJU Int*. 2007;99(5):1154-60.

20. Dolbier Jr WR, Li A-R, Koch CJ, Shiue C-Y, Kachur AV. [18F]-EF5, a marker for PET detection of hypoxia: synthesis of precursor and a new fluorination procedure. *Appl Radiat Isot*. 2001;54(1):73-80.

21. Dubois LJ, Lieuwes NG, Janssen MH, Peeters WJ, Windhorst AD, Walsh JC, et al. Preclinical evaluation and validation of [^{18}F] HX4, a promising hypoxia marker for PET imaging. *Proceedings of the National Academy of Sciences*. 2011;108(35):14620-5.

22. Rasey JS, Hofstrand PD, Chin LK, Tewson TJ. Characterization of [^{18}F]fluoroetanidazole, a new radiopharmaceutical for detecting tumor hypoxia. *J Nucl Med*. 1999;40(6):1072-9.

23. Zha Z, Zhu L, Liu Y, Du F, Gan H, Qiao J, et al. Synthesis and evaluation of two novel 2-nitroimidazole derivatives as potential PET radioligands for tumor imaging. *Nucl Med Biol*. 2011;38(4):501-8.

24. Bejot R, Kersemans V, Kelly C, Carroll L, King RC, Gouverneur V, et al. Pre-clinical evaluation of a 3-nitro-1,2,4-triazole analogue of [^{18}F]FMISO as hypoxia-selective tracer for PET. *Nucl Med Biol*. 2010;37(5):565-75.

25. Vavere AL, Lewis JS. Cu-ATSM: a radiopharmaceutical for the PET imaging of hypoxia. *Dalton trans*. 2007;21(43):4893-902.

26. Lewis JS, McCarthy DW, McCarthy TJ, Fujibayashi Y, Welch MJ. Evaluation of ^{64}Cu-ATSM in vitro and in vivo in a hypoxic tumor model. *J Nucl Med*. 1999;40(1):177-83.

27. Lewis JS, Laforest R, Dehdashti F, Grigsby PW, Welch MJ, Siegel BA. An imaging comparison of ^{64}Cu-ATSM and ^{60}Cu-ATSM in cancer of the uterine cervix. *J Nucl Med*. 2008;49(7):1177-82.

28. Dietz DW, Dehdashti F, Grigsby PW, Malyapa RS, Myerson RJ, Picus J, et al. Tumor hypoxia detected by positron emission tomography with ^{60}Cu-ATSM as a predictor of response and survival in patients undergoing Neoadjuvant chemoradiotherapy for rectal carcinoma: a pilot study. *Dis Colon Rectum*. 2008 ;51(11):1641-8.

29. Lucignani G. PET imaging with hypoxia tracers: a must in radiation therapy. *Eur J Nucl Med Mol Imaging*. 2008;35(4):838-42.

30. Lehtiö K, Eskola O, Viljanen T, Oikonen V, Grönroos T, Sillanmäki L, et al. Imaging perfusion and hypoxia with PET to predict radiotherapy response in head-and-neck cancer. *Int. J. Radiat. Oncol. Biol. Phys.* 2004;59(4):971-82.

31. Kelloff GJ, Hoffman JM, Johnson B, Scher HI, Siegel BA, Cheng EY, et al. Progress and promise of FDG-PET imaging for cancer patient management and oncologic drug development. *Clin. Ca. Res.* 2005;11(8):2785-808.

32. Harry VN, Semple SI, Parkin DE, Gilbert FJ. Use of new imaging techniques to predict tumour response to therapy. *Lancet Oncol* 2010;11(1):92-102.

33. Gambhir SS. Molecular imaging of cancer with positron emission tomography. *Nature Rev. Ca.* 2002;2(9):683-93.

34. de Rosales RTM, Årstad E, Blower PJ. Nuclear imaging of molecular processes in cancer. *Targeted Oncol.* 2009;4(3):183-97.

35. Velikyan I, Maecke H, Langstrom B. Convenient preparation of ^{68}Ga-based PET-radiopharmaceuticals at room temperature. *Bioconjug. Chem.* 2008;19(2):569-73.

36. Jeong JM, Hong MK, Chang YS, Lee Y-S, Kim YJ, Cheon GJ, et al. Preparation of a promising angiogenesis PET imaging agent: ^{68}Ga-labeled c (RGDyK)–isothiocyanatobenzyl-1, 4, 7-triazacyclononane-1, 4, 7-triacetic acid and feasibility studies in mice. *J Nucl Med*. 2008;49(5):830-6.

37. Shetty D, Lee Y-S, Jeong JM. ^{68}Ga-labeled radiopharmaceuticals for positron emission tomography. *Nucl. Med. Mol. Imaging* 2010;44(4):233-40.

38. Shetty D, Jeong JM, Ju CH, Lee Y-S, Jeong SY, Choi JY, et al. Synthesis of novel ^{68}Ga-labeled amino acid derivatives for positron emission tomography of cancer cells. *Nucl. Med. Biol.* 2010;37(8):893-902.

39. Shetty D, Jeong JM, Ju CH, Kim YJ, Lee J-Y, Lee Y-S, et al. Synthesis and evaluation of macrocyclic amino acid derivatives for tumor imaging by gallium-68 positron emission tomography. *Bioorg. Med. Chem.* 2010;18(21):7338-47.

40. Shetty D, Choi SY, Jeong JM, Hoigebazar L, Lee YS, Lee DS, et al. Formation and Characterization of Gallium (III) Complexes with Monoamide Derivatives of 1, 4, 7-Triazacyclononane-1, 4, 7-triacetic Acid: A Study of the Dependency of Structure on Reaction pH. *Eur. J. Inorg. Chem.* 2010;(34):5432-8.

41. Waldron BP, Parker D, Burchardt C, Yufit DS, Zimny M, Roesch F. Structure and stability of hexadentate complexes of ligands based on AAZTA for efficient PET labelling with gallium-68. *Chem. Commun.* 2013;49(6):579-81.

42. Yang BY, Jeong JM, Kim YJ, Choi JY, Lee Y-S, Lee DS, et al. Formulation of ^{68}Ga BAPEN kit for myocardial positron emission tomography imaging and biodistribution study. *Nucl. Med. Biol.* 2010;37(2):149-55.

43. Clarke ET, Martell AE. Stabilities of the Fe(III), Ga(III) and In(III) chelates of N,N′,N″-triazacyclononanetriacetic acid. *Inorganica Chimica Acta*. 1991; 181(2):273-80.

44. Jyo A, Kohno T, Terazono Y, Kawano S. Crystal Structure of Gallium(III) Complex of 1, 4, 7-Triazacyclononane-N, N′, N′-triacetate. *Anal Sci*. 1990;6(2):323-4.

45. Antunes P, Ginj M, Zhang H, Waser B, Baum RP, Reubi JC, et al. Are radiogallium-labelled DOTA-conjugated somatostatin analogues superior to those labelled with other radiometals? *Eur J Nucl Med Mol Imaging*. 2007;34(7):982-93.

46. Breeman WA, de Jong M, de Blois E, Bernard BF, Konijnenberg M, Krenning EP. Radiolabelling DOTA-peptides with ^{68}Ga. *Eur J Nucl Med Mol Imaging*. 2005;32(4):478-85.

47. Singh AN, Liu W, Hao G, Kumar A, Gupta A, Öz OK, et al. Multivalent bifunctional chelator scaffolds for gallium-68 based positron emission tomography imaging probe design: signal amplification via multivalency. *Bioconjug. Chem.* 2011;22(8):1650-62.

48. Notni J, Hermann P, Havlíčková J, Kotek J, Kubíček V, Plutnar J, et al. A Triazacyclononane-Based Bifunctional Phosphinate Ligand for the Preparation of Multimeric 68Ga Tracers for Positron Emission Tomography. *Chem. Eur. J.* 2010;16(24):7174-85.

49. André JP, Maecke HR, Zehnder M, Macko L, Akyel KG. 1, 4, 7-Triazacyclononane-1-succinic acid-4, 7-diacetic acid (NODASA): a new bifunctional chelator for radio gallium-labelling of biomolecules. *Chem. Commun.* 1998 (12):1301-2.

50. Eisenwiener K-P, Prata M, Buschmann I, Zhang H-W, Santos A, Wenger S, et al. NODAGATOC, a new chelator-coupled somatostatin analogue labeled with [$^{67/68}$Ga] and [^{111}In] for SPECT, PET, and targeted therapeutic applications of somatostatin receptor (hsst2) expressing tumors. *Bioconjug. Chem.*2002;13(3):530-41.

51. Prata M, Santos A, Geraldes C, De Lima J. Characterisation of ^{67}Ga 3+ complexes of triaza macrocyclic ligands: biodistribution and clearance studies. *Nucl. Med. Biol.* 1999;26(6):707-10.

52. Prata M, Santos A, Geraldes C, De Lima J. Structural and in vivo studies of metal chelates of Ga (III) relevant to biomedical imaging. *J Inorg Biochem*. 2000;79(1):359-63.

53. Hoigebazar L, Jeong JM, Hong MK, Kim YJ, Lee JY, Shetty D, et al. Synthesis of ^{68}Ga-labeled DOTA-nitroimidazole derivatives and their feasibilities as hypoxia imaging PET tracers. *Bioorg. Med. Chem.* 2011;19(7):2176-81.

54. Hoigebazar L, Jeong JM, Choi SY, Choi JY, Shetty D, Lee Y-S, et al. Synthesis and characterization of nitroimidazole derivatives for ^{68}Ga-labeling and testing in tumor xenografted mice. *J. Med. Chem.* 2010;53(17):6378-85.

55. Hoigebazar L, Jeong JM, Lee J-Y, Shetty D, Yang BY, Lee Y-S, et al. Syntheses of 2-Nitroimidazole Derivatives Conjugated with 1, 4, 7-Triazacyclononane-N, N′-Diacetic Acid Labeled with F-18 Using an Aluminum Complex Method for Hypoxia Imaging. *J. Med. Chem.*. 2012;55(7):3155-62.

56. Huang H, Zhou H, Li Z, Wang X, Chu T. Effect of a second nitroimidazole redox centre on the accumulation of a hypoxia marker: synthesis and in vitro evaluation of ^{99m}Tc-labeled bisnitroimidazole propylene amine oxime complexes. *Bioorg Med Chem Lett.* 2012;22(1):172-7.

57. Mei L, Wang Y, Chu TW. ^{99m}Tc/Re complexes bearing bisnitroimidazole or mononitroimidazole as potential bioreductive markers for tumor: Synthesis, physicochemical characterization and biological evaluation. *Eur J Med Chem*. 2012;58:50-63.

58. Notni J, Šimeček J, Hermann P, Wester HJ. TRAP, a Powerful and Versatile Framework for Gallium-68 Radiopharmaceuticals. *Chem. Eur. J.* 2011;17(52):14718-22.

59. Gomez FLG, Uehara T, Rokugawa T, Higaki Y, Suzuki H, Hanaoka H, et al. Synthesis and Evaluation of Diastereoisomers of 1, 4, 7-Triazacyclononane-1, 4, 7-tris-(glutaric acid)(NOTGA) for Multimeric Radiopharmaceuticals of Gallium. *Bioconjug. Chem.* 2012;23(11):2229-38.

60. Notni J, Pohle K, Wester HJ. Be spoilt for choice with radiolabelled RGD peptides: preclinical evaluation of ^{68}Ga-TRAP(RGD)(3). *Nucl Med Biol*. 2013;40(1):33-41.

61. Jeong JM, Kim YJ, Lee YS, Lee DS, Chung JK, Lee MC. Radiolabeling of NOTA and DOTA with positron emitting ^{68}Ga and investigation of in vitro properties. *Nucl. Med. Mol. Imaging* 2009;43(4):330-6.

62. Lee JJ, Shetty D, Lee YS, Kim SE, Kim YJ, Hong MK, et al. Evaluation of ^{111}In-labeled macrocyclic chelator-amino acid

derivatives for cancer imaging. *Nucl. Med. Biol*. 2012; 39(3):325-33.

63. Kumar P, Stypinski D, Xia H, McEwan AJB, Machulla HJ, Wiebe LI. Fluoroazomycin arabinoside (FAZA): synthesis, 2H and 3H-labelling and preliminary biological evaluation of a novel 2-nitroimidazole marker of tissue hypoxia. *J Labelled Compd Radiopharm*. 1999;42(1):3-16.

64. Kelada OJ, Carlson DJ. Molecular imaging of tumor hypoxia with positron emission tomography. Radiat Res. 2014;181(4):335-49.

65. Krohn KA, Link JM, Mason RP. Molecular imaging of hypoxia. *J Nucl Med*. 2008, *49 Suppl 2*, 129S.

Appendix

Spectral Analysis Results

^{1}H NMR Spectra

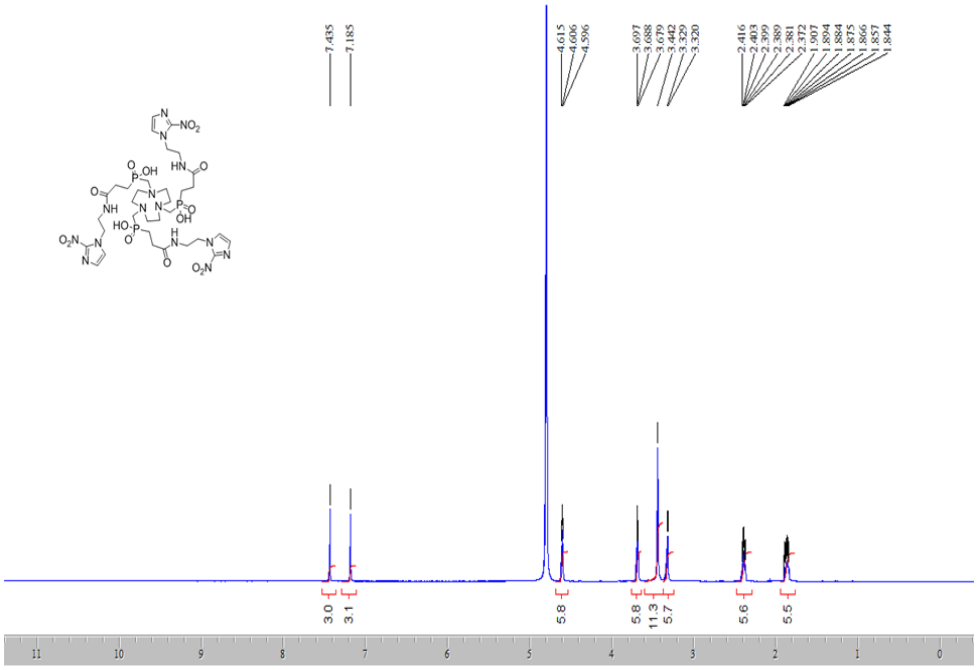
7.435
7.185
4.615
4.606
4.596
3.697
3.688
3.679
3.442
3.329
3.320
2.416
2.403
2.399
2.389
2.381
2.372
1.907
1.894
1.884
1.875
1.866
1.857
1.844
3.0
3.1
5.8
5.8
11.3
5.7
5.6
5.5

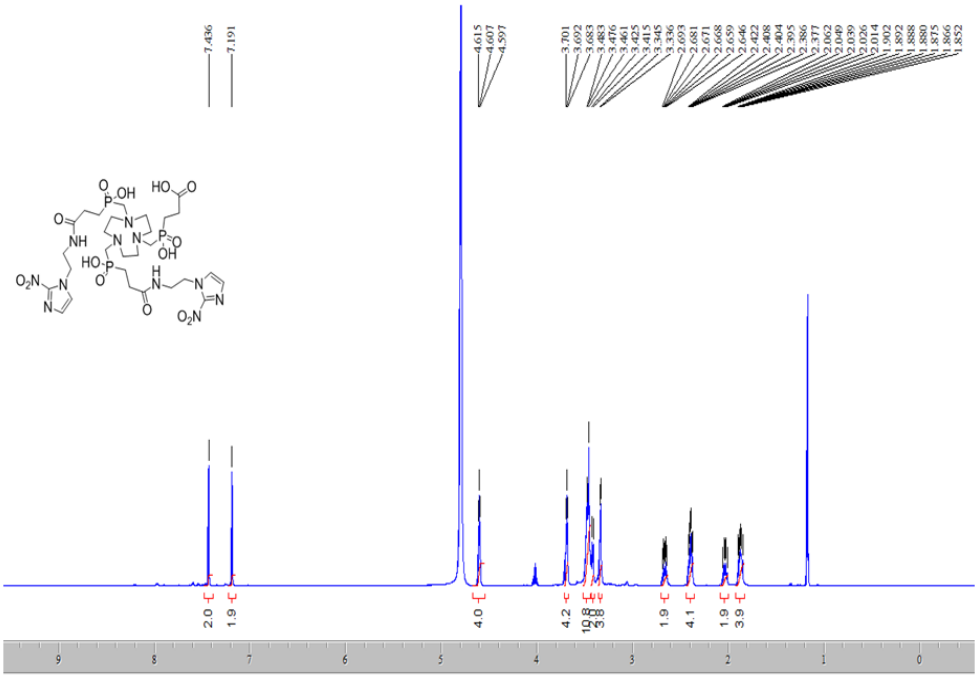
7.436
7.191
4.615
4.607
4.597
3.701
3.692
3.683
3.483
3.476
3.461
3.425
3.415
3.345
3.336
2.693
2.681
2.671
2.668
2.659
2.646
2.422
2.408
2.404
2.395
2.386
2.377
2.062
2.049
2.039
2.026
2.014
1.902
1.892
1.888
1.880
1.875
1.866
1.852
2.0
1.9
4.0
4.2
1.9
4.1
1.9
3.9

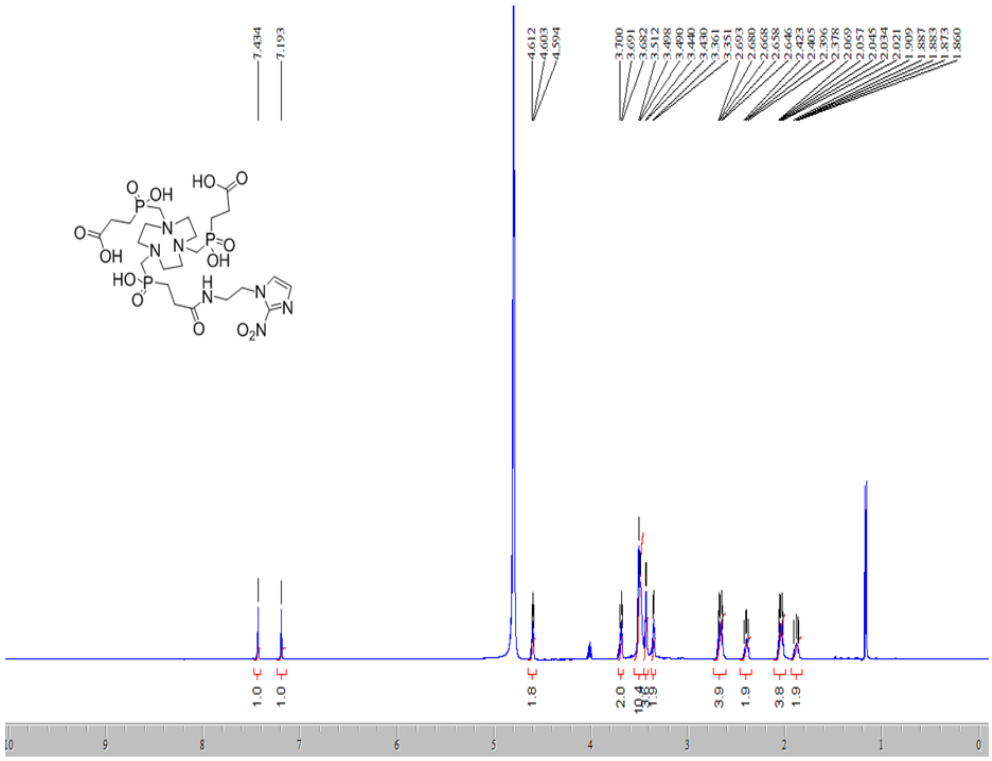
7.434
7.193
4.612
4.603
4.594
3.700
3.691
3.682
3.512
3.498
3.490
3.440
3.430
3.361
3.351
2.693
2.680
2.668
2.658
2.646
2.483
2.465
2.396
2.378
2.069
2.057
2.045
2.034
2.021
1.909
1.887
1.883
1.873
1.860
1.0
1.0
1.8
2.0
10.4
1.8
3.9
1.9
3.8
1.9
10
9
8
7
6
5
4
3
2
1
0

^{13}C NMR Spectra

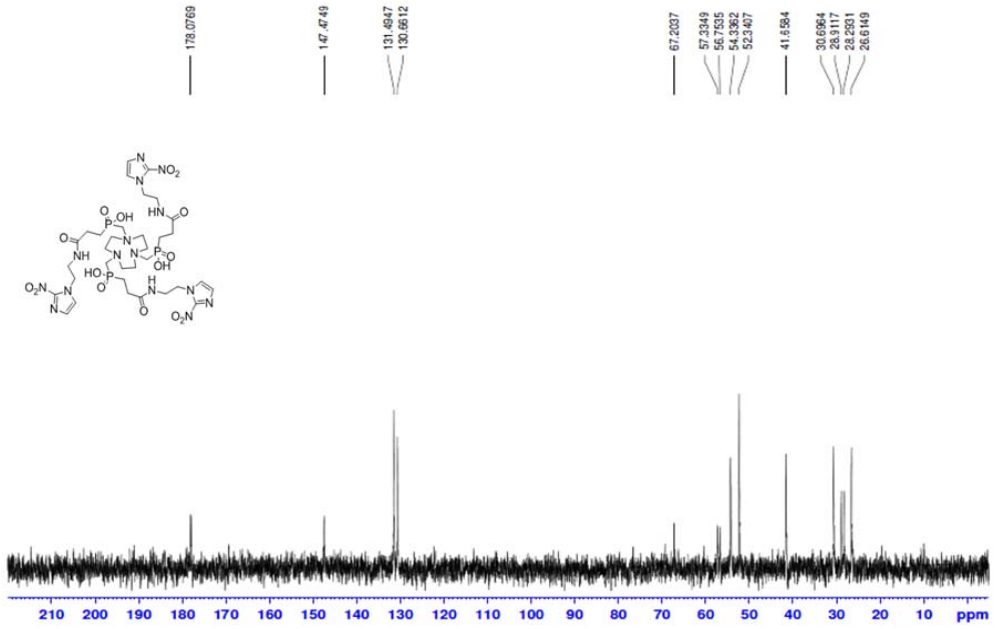
178.0769
147.4749
131.4947
130.6612
67.2037
57.3349
56.7535
54.3362
52.3407
41.6584
30.6964
28.9117
28.2291
26.6149
210 200 190 180 170 160 150 140 130 120 110 100 90 80 70 60 50 40 30 20 10 ppm

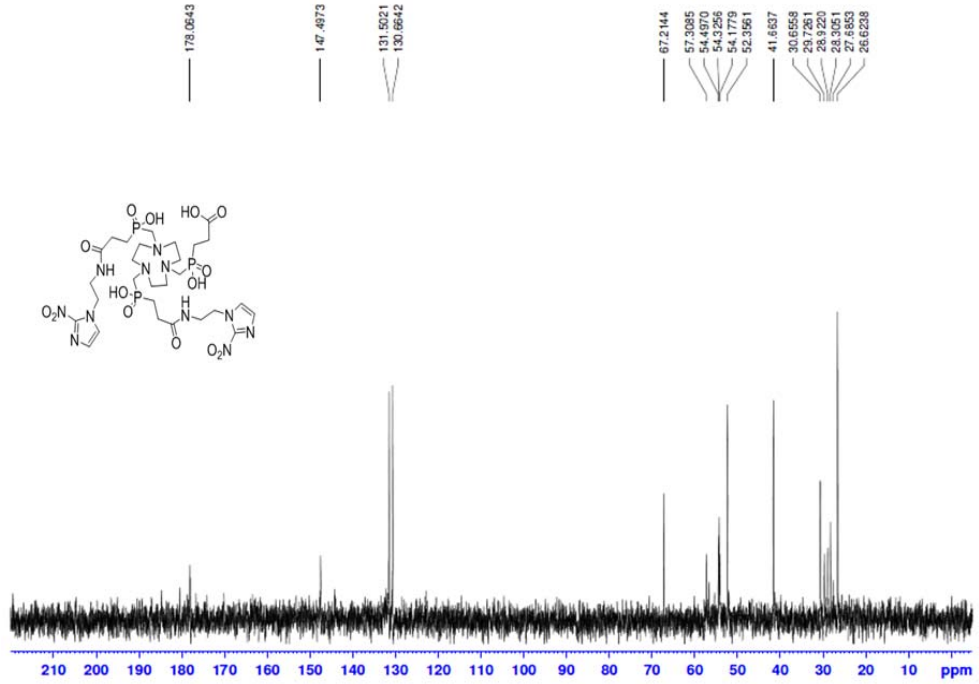
178.0643
147.4973
131.5021
130.6642
67.2144
57.3085
54.4970
54.3256
54.1779
52.3561
41.6637
30.6558
29.7261
28.9220
28.3051
27.6853
26.6238
210 200 190 180 170 160 150 140 130 120 110 100 90 80 70 60 50 40 30 20 10 ppm

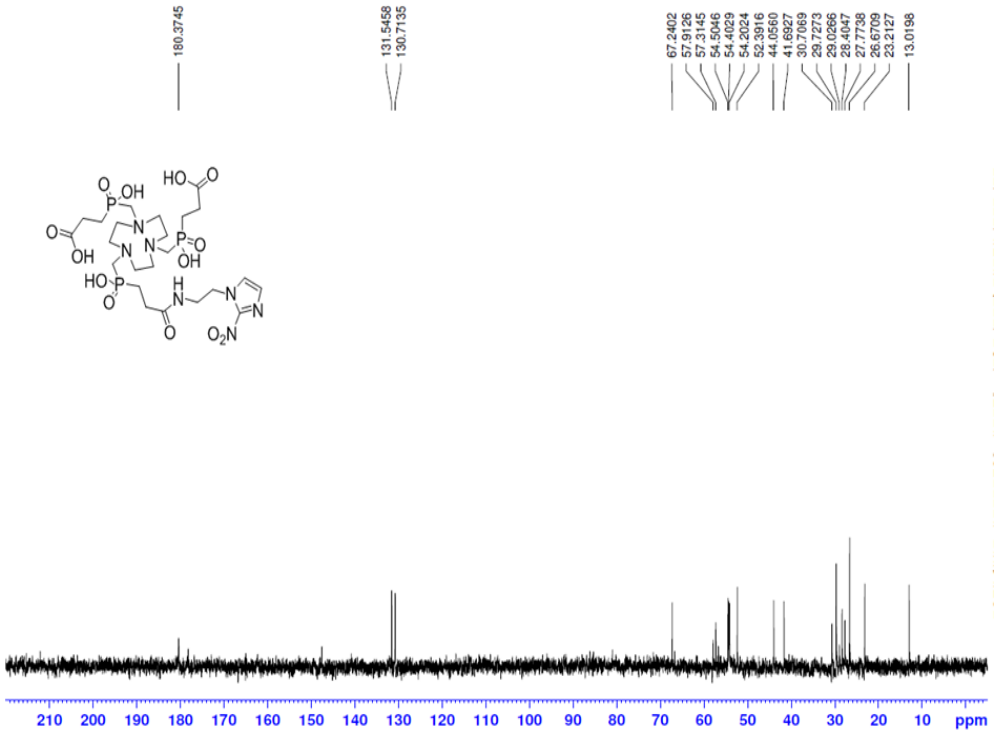
180.3745
131.5458
130.7135
67.2402
57.9126
57.3145
54.5046
54.4029
54.2024
52.3916
44.0560
41.6927
30.7069
29.7273
29.0266
28.4047
27.7738
26.6709
23.2127
13.0198
210 200 190 180 170 160 150 140 130 120 110 100 90 80 70 60 50 40 30 20 10 ppm

^{31}P NMR Spectra

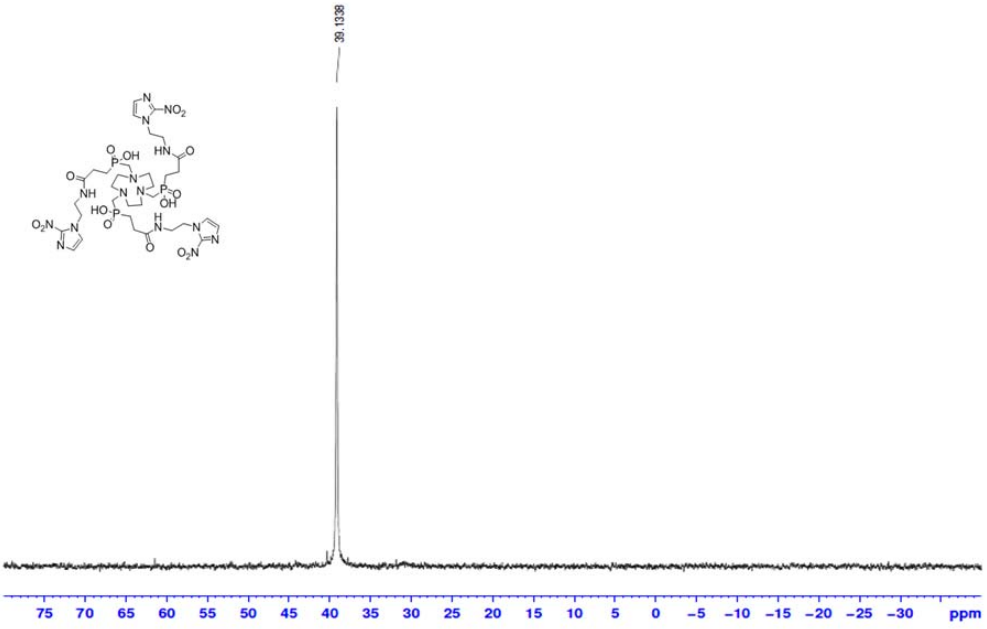
39.1338
75 70 65 60 55 50 45 40 35 30 25 20 15 10 5 0 -5 -10 -15 -20 -25 -30 ppm

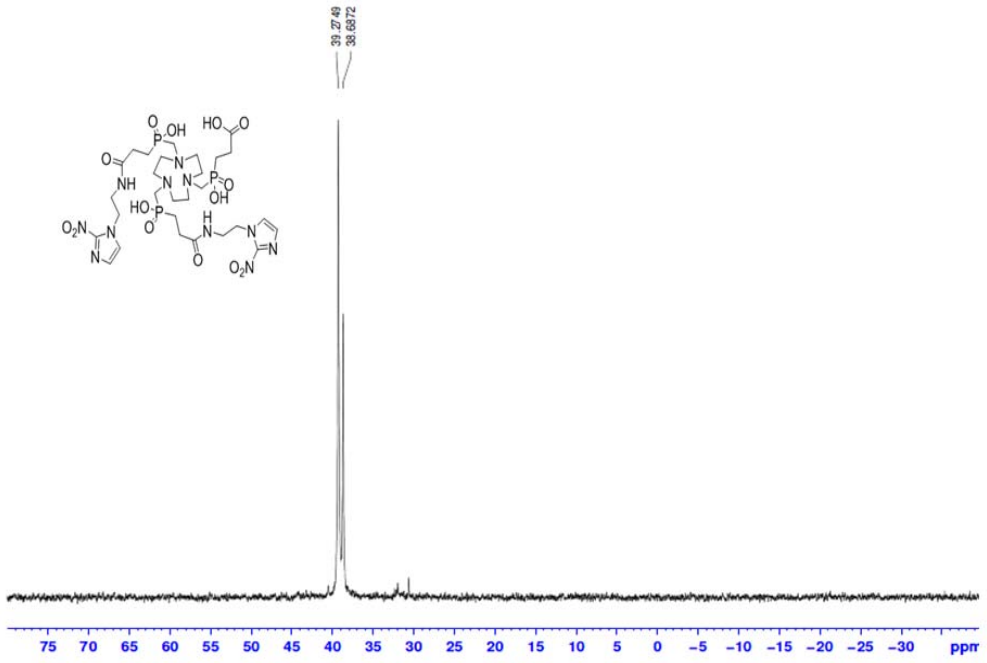
39.2749
38.6872
75 70 65 60 55 50 45 40 35 30 25 20 15 10 5 0 -5 -10 -15 -20 -25 -30 ppm

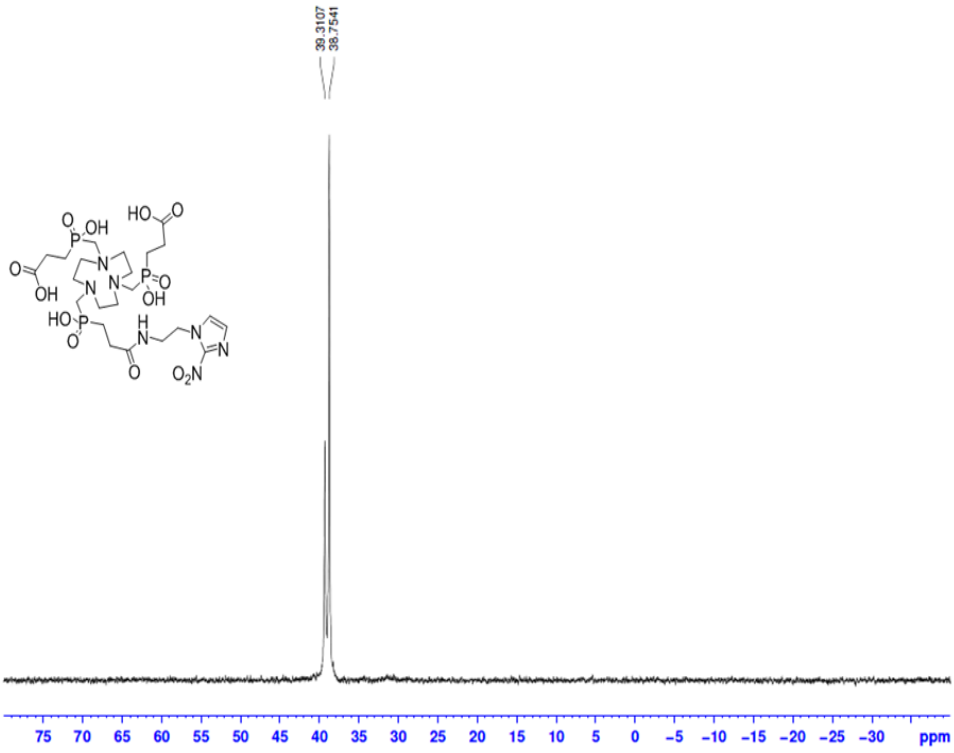
39.3107
38.7541
75 70 65 60 55 50 45 40 35 30 25 20 15 10 5 0 −5 −10 −15 −20 −25 −30 ppm

Mass Spectra

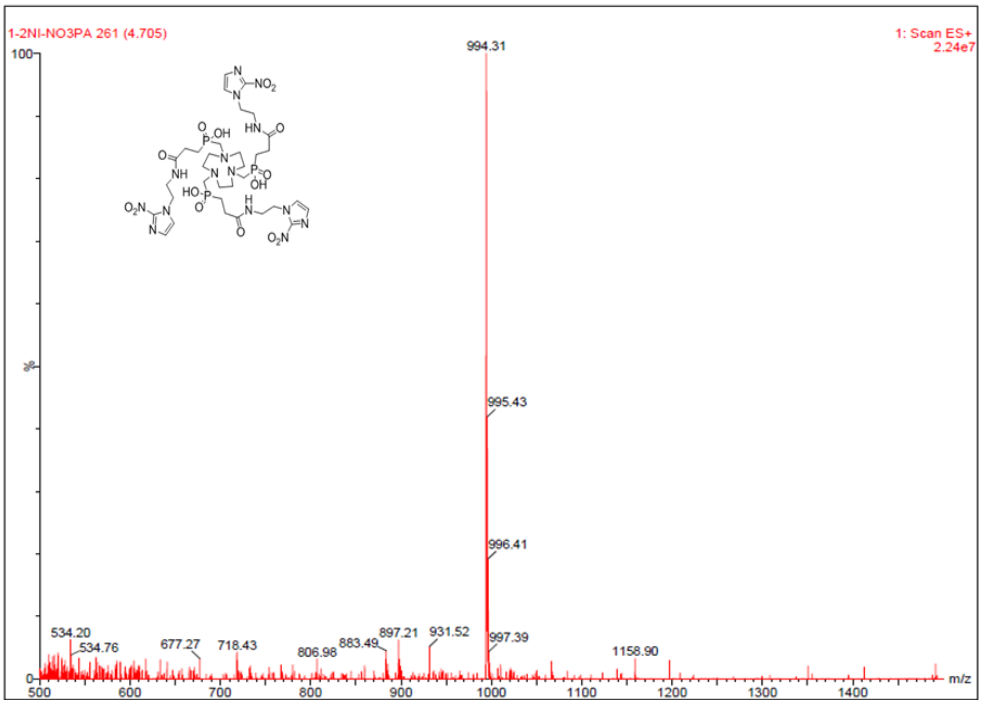
1-2NI-NO3PA 261 (4.705)
1: Scan ES+
2.24e7
100
%
0
994.31
995.43
996.41
997.39
534.20
534.76
677.27
718.43
806.98
883.49
897.21
931.52
1158.90
m/z
500
600
700
800
900
1000
1100
1200
1300
1400

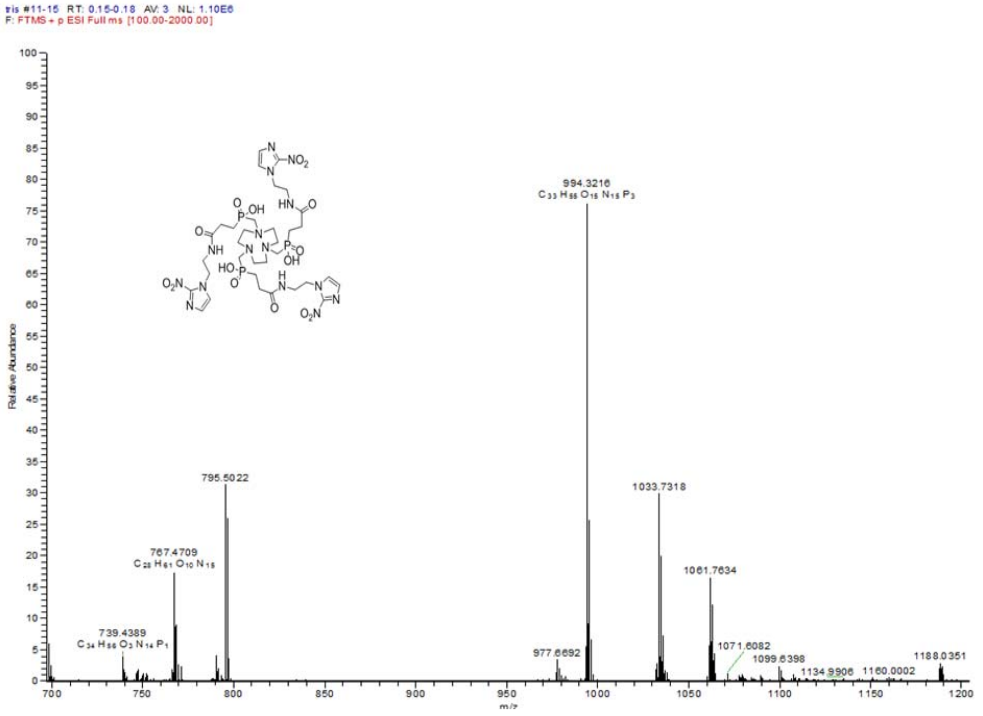
tris #11-15 RT: 0.15-0.18 AV: 3 NL: 1.10E6
F: FTMS + p ESI Full ms [100.00-2000.00]
Relative Abundance
994.3216
C33 H58 O15 N15 P3
795.5022
1033.7318
767.4709
C28 H51 O10 N15
1061.7634
739.4389
C34 H56 O3 N14 P1
977.6692
1071.6082
1099.6398
1134.9906
1160.0002
1188.0351
m/z

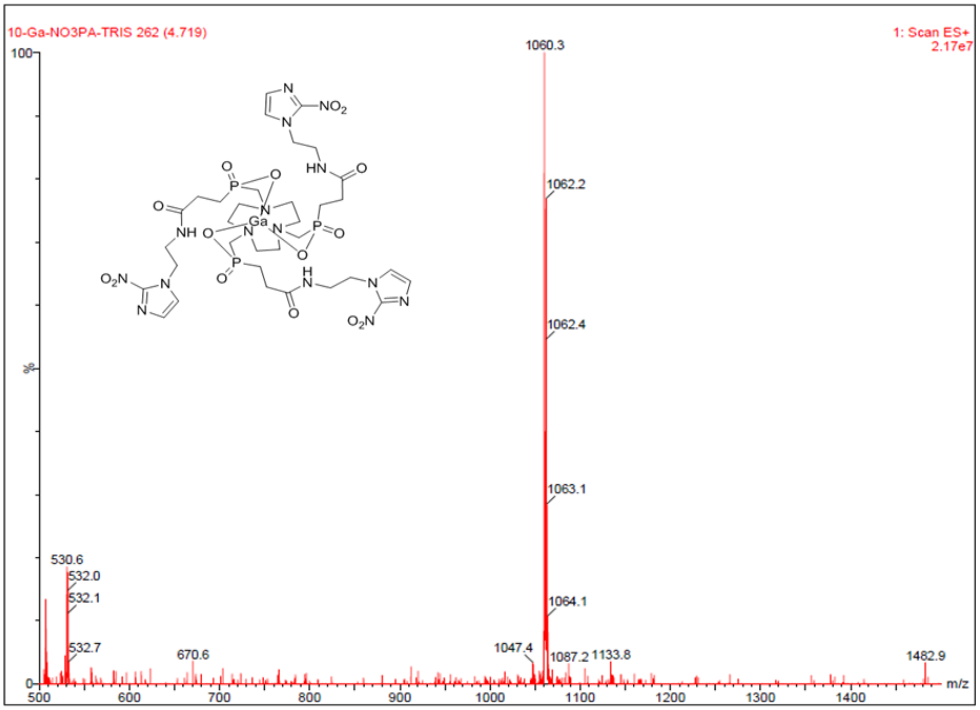
10-Ga-NO3PA-TRIS 262 (4.719)
1: Scan ES+
2.17e7
100
%
0
1060.3
1062.2
1062.4
1063.1
1064.1
530.6
532.0
532.1
532.7
670.6
1047.4
1087.2
1133.8
1482.9
500
600
700
800
900
1000
1100
1200
1300
1400
m/z

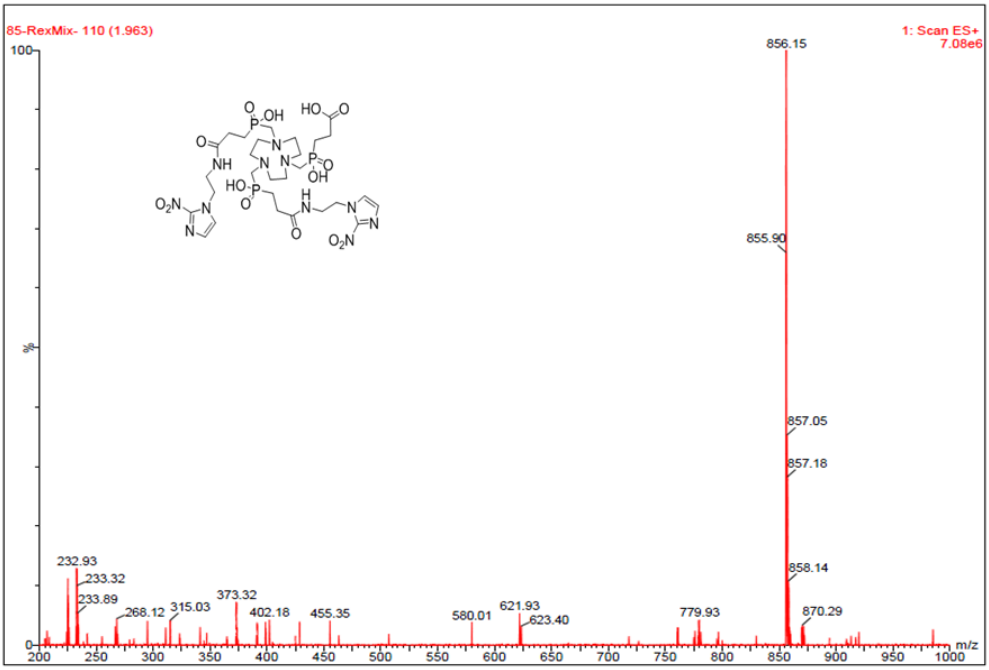
85-RexMix- 110 (1.963)
1: Scan ES+
7.08e6
100
%
0
856.15
855.90
857.05
857.18
858.14
870.29
232.93
233.32
233.89
268.12
315.03
373.32
402.18
455.35
580.01
621.93
623.40
779.93
200
250
300
350
400
450
500
550
600
650
700
750
800
850
900
950
1000
m/z

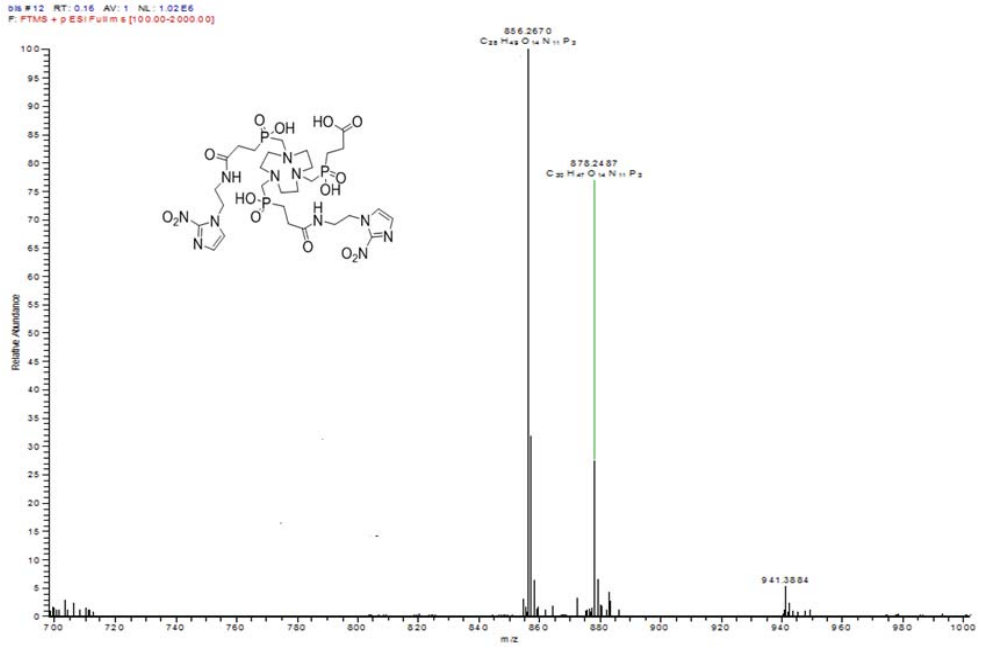
Relative Abundance
m/z
856.2670
878.2487
941.3884

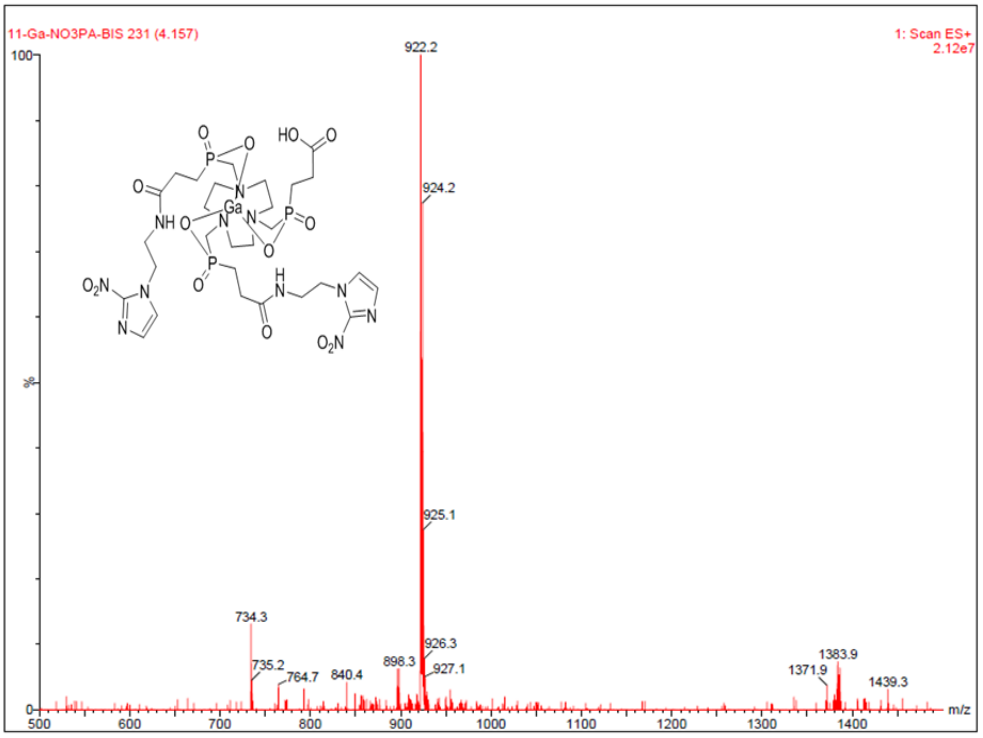
11-Ga-NO3PA-BIS 231 (4.157)
1: Scan ES+
2.12e7
%
m/z
922.2
924.2
925.1
926.3
927.1
734.3
735.2
764.7
840.4
898.3
1371.9
1383.9
1439.3

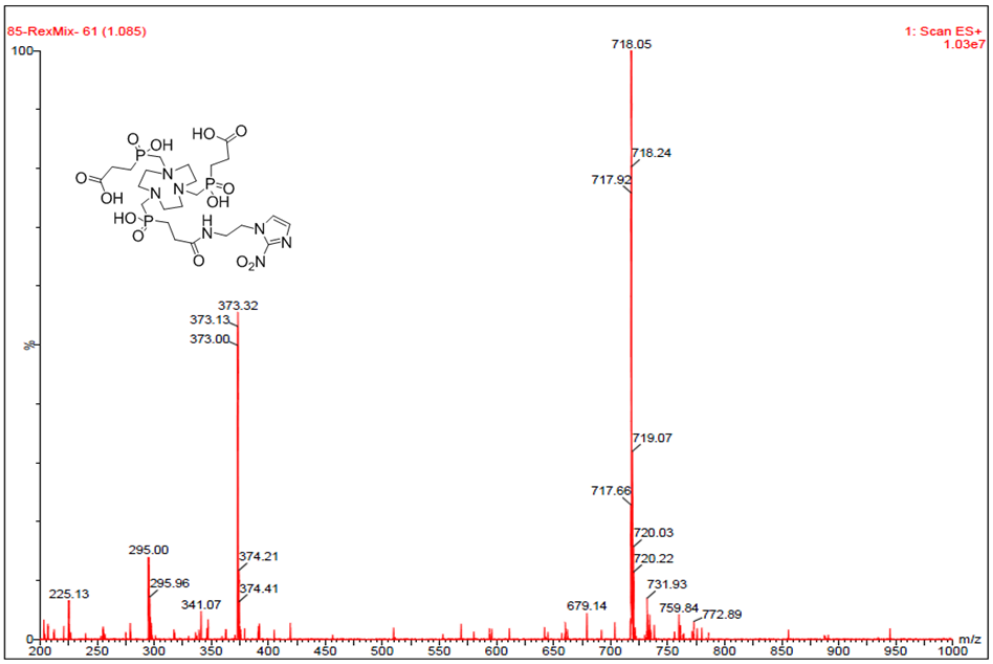
85-RexMix- 61 (1.085)
1: Scan ES+
1.03e7
718.05
718.24
717.92
373.32
373.13
373.00
719.07
717.66
720.03
720.22
731.93
759.84
772.89
295.00
374.21
295.96
374.41
225.13
341.07
679.14
%
m/z

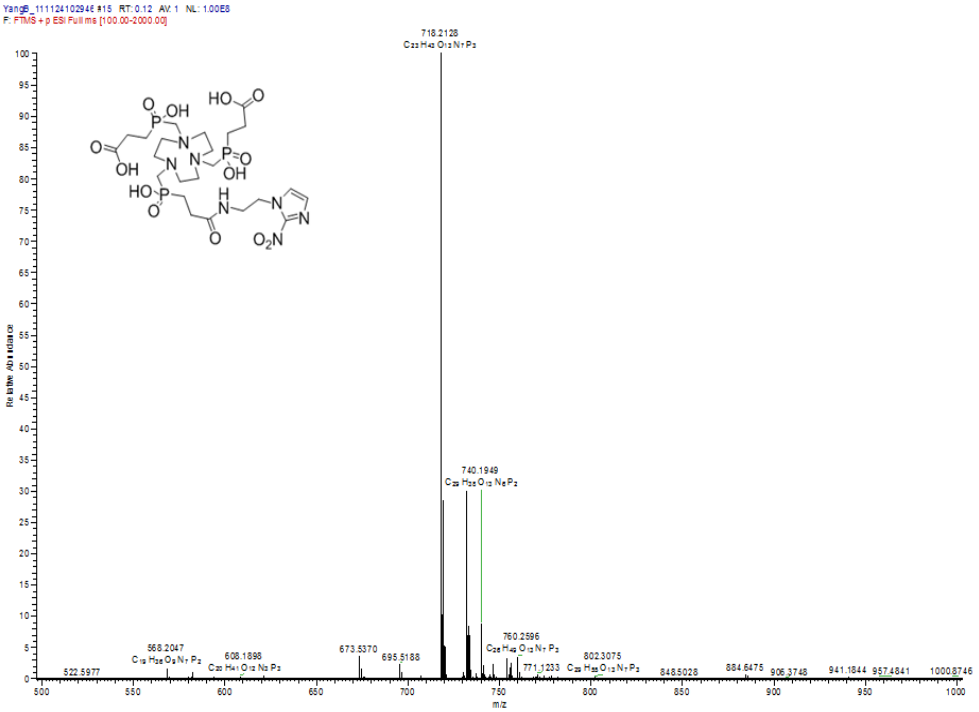
718.2128
740.1949
760.2596
568.2047
608.1898
673.5370
695.5188
522.5977
771.1233
802.3075
848.5028
884.6475
906.3748
941.1844
957.4841
1000.8746
Relative Abundance
m/z

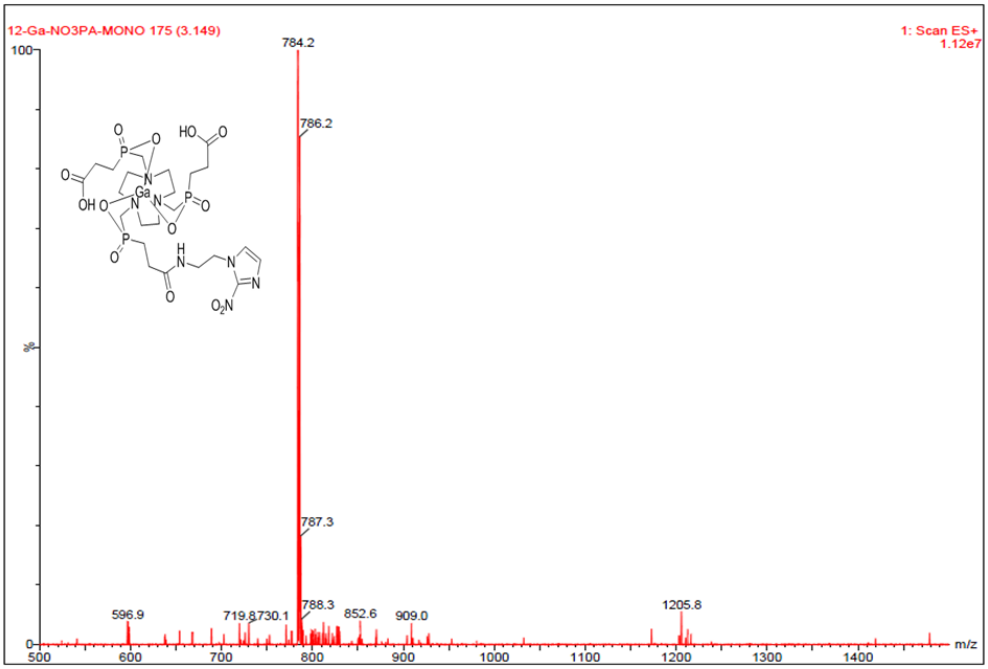
12-Ga-NO3PA-MONO 175 (3.149)
1: Scan ES+
1.12e7
100
%
0
784.2
786.2
787.3
788.3
596.9
719.8
730.1
852.6
909.0
1205.8
500
600
700
800
900
1000
1100
1200
1300
1400
m/z

Abstract in Korean

방사성 표지 니트로이미다졸 (NI) 유도체는 저산소증 영상 분야에서 광범위하게 연구되어 오고 있다. 본 연구에서는 특별히 저산소 조직에 대한 흡수를 높이기 위해 킬레이트화제 TRAP 에 모노-, 비스-, 트리스니트로이미다졸을 결합시킨 68 갈륨 표지화물을 개발하였고 이에 대한 결과들을 소개를 하고 있다.

세 가지 표지화물 모두 높은 방사표지 효율 (>96%)을 보였으며 준비한 매질 내 상온과 37 ° C 사람 혈청에서 모두 4 시간까지 안정한 것으로 나타났다. 생체 외 세포 흡수 실험에 의하면 3 가 화합물이 가장 높은 저산소 대비 정상세포 흡수비율 ($p < 0.005$)을 보였다. 이종 이식한 CT26 종양 조직에서의 저산소증은 면역조직화학적 분석으로 확인하였다. CT26 이종 이식한 쥐를 이용한 생체분포 실험에서 3 가 유도체가 암 세포에 가장 많이 흡수되었다 (^{68}Ga-3: 0.17 ± 0.04, ^{68}Ga-4: 0.33 ± 0.04, ^{68}Ga-5: 0.45 ± 0.09, and ^{68}Ga-6: 0.47 ± 0.05% ID/g). 모든 니트로이미다졸 유도체가 대조 화합물과 비교하여 1 시간 주사 후 암 세포에 유의미한 높은 흡수율을 보였다. CT26 이종 이식한 쥐를 이용한

소동물 양전자단층촬영 (PET) 연구에서 3 가 유도체는 또한 주사 후 1 시간 뒤 암세포에 대해 가장 높은 표준섭취화계수 (SUV) 를 보였다 (^{68}Ga-3: 0.10 ± 0.06; ^{68}Ga-4: 0.20 ± 0.06; ^{68}Ga-5: 0.33 ± 0.08; ^{68}Ga-6: 0.59 ± 0.09). 결론적으로 저산소증 영상을 위한 다가 68 갈륨 표지 니트로이미다졸 유도체들을 성공적으로 합성하였으며, 그 중 3 가 화합물이 생체 내 분포 실험과 양전자단층촬영 연구에서 가장 높은 암 세포 흡수를 보였다.

키워드 : trisnitroimidazole; bisnitroimidazole; **다 자리; 갈륨-68; 저산소증; 양전자단층촬영.**

학번: 2010-31372